Glauber-eikonal study of electron-molecule scattering at intermediate energies with the use of the free-electron-gas model: H_2

P. K. Bhattacharyya and D. K. Syamal
Department of Physics, Calcutta University, 92 Acharyya Prafulla Chandra Road, Calcutta 700009, West Bengal, India

B. C. Saha
Department of Physics and Astronomy, The University of Oklahoma, Norman, Oklahoma 73019
(Received 12 October 1984)

An improved version of the Glauber-eikonal amplitude for electron-molecule scattering, originally developed by Bhattacharyya and Ghosh, that includes the effects of nonspherical potential terms up to $\nu=6$ is presented. Application is made to e-H_2 scattering at intermediate energies to test a recently proposed, parameter-free, correlation-polarization potential. This potential is based, as suggested by O'Connell and Lane, on the hybridization of local-electron-gas theory and the long-range polarization. Results obtained are found to be very encouraging.

I. INTRODUCTION

In one of the first attempts[1,2] of the application of the Glauber approximation[3] to intermediate-energy electron scattering by molecular targets Bhattacharyya and Ghosh[2] considered the one-center expansion of the effective electron-molecule potential and obtained the Glauber scattering amplitude in terms of a series in products of Bessel functions. This amplitude for a fixed molecular orientation is then utilized, in the framework of adiabatic approximation,[4,5] to derive average elastic (sum of pure elastic and rotational excitation) and state-to-state rotational-excitation cross sections. Following this method, we made a systematic study of electron scattering by molecular hydrogen,[2,6,7] nitrogen,[8] and oxygen[9] and positron scattering by a hydrogen molecule.[10] Recently, Bhattacharyya and Syamal[11] obtained the Glauber-eikonal amplitude for an effective complex potential in order to study the effects of electronic excitations on rotational excitations of the hydrogen molecule. All these studies have revealed that the Glauber-eikonal scattering amplitude is quite effective in reproducing different experimental cross sections. But the method of Bhattacharyya and Ghosh[2,6] for real electron- (position-) molecule potentials and that of Bhattacharyya and Syamal[11] for complex electron-molecule potential suffer from a serious limitation. In the one-center expansion of the effective electron- (positron) molecule potential in terms of Legendre polynomial P_ν they considered terms up to $\nu=2$. But such an expansion is very slowly convergent about the nuclei, and neglect of nonspherical terms represented by $\nu>2$ makes the computed cross sections unconverged with respect to the asphericity of the electron- (positron-) molecule potential. That the inclusion of nonspherical potentials with $\nu>2$ affects the calculated cross sections significantly is evident from the unconverged[12] and converged[13] close-coupling studies of e-N_2 scattering at intermediate energies by Truhlar and co-workers. Thus it is obvious that if this shortcoming could be eliminated, at least to a certain extent by including a few more nonspherical terms in the derivation of Glauber amplitude, the potentiality of this amplitude in describing electron- (positron-) molecule scattering at intermediate energies could be properly assessed and reliable cross sections could be provided.

Furthermore, in all previous calculations[7-10] simple parameter-dependent model potentials have been used to represent the electron- (positron-) molecule interaction, which, in the state-of-the-art context, could be much improved. Recently O'Connell and Lane[14] suggested a nonadjustable model for electron scattering that includes exchange and correlation effects in a hybridization of local-electron-gas theory and long-range polarization. Padial and Norcross[15] calculated the hybrid correlation-polarization potential for several molecules including polar molecules. They obtained encouraging results for e-H_2 and e-N_2 scattering at low energies. It would be interesting to test this model also for intermediate-energy electron scattering.

Accordingly, we derived in the present paper the Glauber-eikonal scattering amplitude, which includes nonspherical one-center expansion terms up to $\nu=6$, for linear molecules possessing $D_{\infty h}$ symmetry. We have considered the real part of the effective potential and the target molecule is assumed to be in ground electronic and vibrational states. Application is made to e-H_2 scattering for incident energies 20—400 eV. In an earlier study Bhattacharyya *et al.*[7] used the *ab initio* polarization potential of Henry and Lane[16] and the parameter-dependent polarization potential of Hara.[17] The static and the spherical part of the exchange[17] potentials were generated by using the Wang[18] wave function. In contrast, we used here more accurate Fraga-Ransil[19] wave functions to calculate the static, exchange, and correlation-polarization potentials. To test the correlation-polarization potential we compared the cross sections involving this potential with those involving the Henry-Lane polarization potential and also with the available experimental data.

II. SCATTERING AMPLITUDE AND CROSS SECTIONS

We assume that the linear molecule used as a target is in ground electronic and vibrational states so that the target may be treated as a rigid rotor. Then the target wave functions are the spherical harmonics $Y_{jm}(\hat{\mathbf{R}})$. The incident electron with position vector $\mathbf{r}$ interacts with the target through the potential $V(\mathbf{r},\hat{\mathbf{R}})$, where $\hat{\mathbf{R}}$ is the unit vector along the internuclear separation $\mathbf{R}$. In the intermediate-energy region the adiabatic approximation[4,5,20] can be assumed to be valid;[21] then the knowledge of $f(\theta,\hat{\mathbf{R}})$, the elastic scattering amplitude for a fixed molecular orientation of $\mathbf{R}$ for the scattering angle θ, would readily give[20] the state-to-state differential scattering cross section (DCS) $I(j\rightarrow j',\theta)$ for the rotational-excitation process $j\rightarrow j'$ and the average elastic DCS (pure elastic plus all rotational excitation) $\langle I(\theta)\rangle$.

In the present paper we used Glauber-eikonal amplitude for $f(\theta,\hat{\mathbf{R}})$ which is given by (we use atomic units throughout)

$$f(\theta,\hat{\mathbf{R}})=-\frac{ik_i}{2\pi}\int_{b,\phi_r} e^{iqb\cos\phi_r}(e^{-i\chi(b,\hat{\mathbf{R}})}-1)b\,db\,d\phi_r \tag{1}$$

with

$$\chi(b,\hat{\mathbf{R}})=\frac{1}{v_i}\int_{-\infty}^{\infty} V(\mathbf{r},\hat{\mathbf{R}})dz\ , \tag{2}$$

$$\mathbf{r}=\mathbf{b}+\hat{\mathbf{k}}_i z\ .$$

In the above expression $m_e\mathbf{v}_i=\hbar\mathbf{k}_i$ is the momentum of the incident electron, $\mathbf{q}=\mathbf{k}_i-\mathbf{k}_f$ is the momentum transfer to the target, and $\mathbf{b}$ is the impact-parameter vector. The center of mass of the target molecule is taken to be the origin, while the direction of $\mathbf{k}_i$ the polar axis.

We consider $f(\theta,\hat{\mathbf{R}})$ as a sum of two contributions,

$$f(\theta,\hat{\mathbf{R}})=f^{b_0}(\theta,\hat{\mathbf{R}})+f^{\infty}(\theta,\hat{\mathbf{R}})\ , \tag{3}$$

where $f^{b_0}(\theta,\hat{\mathbf{R}})$ is the contribution arising from $b=0$ to $b=b_0$ and $f^{\infty}(\theta,\hat{\mathbf{R}})$ from $b=b_0$ to $b=\infty$. We shall define b_0 later on, but the basic criterion for b_0 is that $\chi(b,\hat{\mathbf{R}})\ll 1$ for $b\geq b_0$.

For linear molecules the effective electron-molecule potential $V(\mathbf{r},\hat{\mathbf{R}})$ in Eq. (2) can be expanded in terms of Legendre polynomials as

$$V(\mathbf{r},\hat{\mathbf{R}})=\sum_{\nu=0}^{\nu_{\max}} V^{\nu}(r)P_{\nu}(\hat{\mathbf{r}}\cdot\hat{\mathbf{R}})\ . \tag{4}$$

$\nu=\nu_{\max}$ is the highest-order term at which the one-center expansion (4) is made to terminate to achieve proper convergence. With the use of (4) and the addition theorem for $P_{\nu}(\hat{\mathbf{r}}\cdot\hat{\mathbf{R}})$, Eq. (2) becomes

$$\chi(b,\hat{\mathbf{R}})=\sum_{\nu=0}^{\nu_{\max}}\sum_{\gamma=0}^{\nu}\delta_{\gamma}\frac{(\nu-|\gamma|)!}{(\nu+|\gamma|)!}I^{\nu,\gamma}(b)P_{\nu}^{|\gamma|}(\cos\theta_R)\times\cos[\gamma(\phi_r-\phi_R)]\ , \tag{5}$$

where

$$I^{\nu,\gamma}(b)=\frac{1}{v_i}\int_{-\infty}^{\infty} V^{\nu}(r)P_{\nu}^{|\gamma|}(\cos\theta_r)dz\ ,$$

$$\delta_{\gamma}=\begin{cases}1 & \text{for } \gamma=0\ ,\\ 2 & \text{for } \gamma\neq 0\ .\end{cases} \tag{6}$$

Here (θ_R,ϕ_R) defines the orientation of the molecular axis with respect to the polar axis. For molecules belonging to point group $D_{\infty h}$, ν is even, including zero, and the integral (6) vanishes for odd values of γ. Thus collecting the terms corresponding to the same values of γ for different ν and setting $\gamma=2n$ and $\nu=2l$, Eq. (5) can be written as

$$\chi(b,\hat{\mathbf{R}})=\sum_{n=0}^{l_{\max}} X^{2n}(b,\theta_R)\cos[2n(\phi_r-\phi_R)] \tag{7}$$

with

$$X^{2n}(b,\theta_R)=\delta_{2n}\sum_{l=n}^{l_{\max}}\frac{(2l-|2n|)!}{(2l+|2n|)!}P_{2l}^{|2n|}(\cos\theta_R)I^{2l,2n}(b)\ , \tag{8}$$

$$I^{2l,2n}(b)=\frac{2}{v_i}\int_0^{\infty} V^{2l}(r)P_{2l}^{|2n|}(\cos\theta_r)dz\ . \tag{9}$$

In the present paper we set $l_{\max}=3$ in the above expression which corresponds to $\nu_{\max}=6$ in Eq. (4). Considering Eqs. (1), (3), and (7), the ϕ_r integration in $f(\theta,\hat{\mathbf{R}})$ can be readily performed. For $f^{b_0}(\theta,\hat{\mathbf{R}})$, we follow Bhattacharyya and Ghosh[6,7] to obtain

$$f^{b_0}(\theta,\hat{\mathbf{R}})=-ik_i\sum_{n=0}^{\infty} f_{2n}^{b_0}(\theta,\theta_R)\cos(2n\phi_R)\ , \tag{10}$$

where

$$f_{2n}^{b_0}(\theta,\theta_R)=\begin{cases}\displaystyle\int_0^{b_0} J_0(qb)\left[\tfrac{1}{2}C\sum_{p,q=0}A_{pq}-1\right]d\,db & \text{for } n=0 \quad (10')\\ \displaystyle\tfrac{1}{2}\int_0^{b_0} CJ_{2n}(qb)\sum_{p,q=0}B_{npq}b\,db & \text{for } n\neq 0\ , \quad (10'')\end{cases}$$

$$A_{pq}=i^{p}\delta_p\delta_q J_p(X^4)J_q(X^6)[J_{n_1}(X^2)+J_{n_2}(X^2)]\ ,$$

$$B_{npq}=i^{n+p}\delta_p\delta_q J_p(X^4)J_q(X^6)\times[J_{n+n_1}(X^2)+J_{n+n_2}(X^2)+(-1)^q J_{n-n_1}(X^2)+(-1)^q J_{n-n_2}(X^2)] \tag{10'''}$$

and

$$n_1=3q+2p\ ,$$

$$n_2=3q-2p\ ,$$

$$C=e^{-iX^0(b,\theta_R)}\ .$$

In the case of $f^{\infty}(\theta,\hat{\mathbf{R}})$, $\chi(b,\hat{\mathbf{R}})\ll 1$ and by making use of the expansion $e^x\simeq 1+x$ we get on ϕ_r integration

$$f^{\infty}(\theta,R)=-k_i\sum_{n=0}^{l_{\max}} f_{2n}^{\infty}(b,\theta_R)\cos(2n\phi_R) \tag{11}$$

with

$$f_{2n}^{\infty}(b,\theta_R)=(-1)^n\int_{b_0}^{\infty} X^{2n}(b,\theta_R)J_{2n}(qb)b\,db\ . \tag{11'}$$

It is to be noted that $f^{\infty}(\theta,\hat{\mathbf{R}})$ is always real and number of terms n is governed by $\nu_{\max}=2l_{\max}$ at which truncation is made for the electron-molecule potential. Remembering these aspects of $f^{\infty}(\theta,\hat{\mathbf{R}})$, Eqs. (10) and (11) can be written as

$$f(\theta,\hat{\mathbf{R}})=-ik_i\sum_{n=0} f_{2n}(\theta,\theta_R)\cos(2n\phi_R)\ , \tag{12}$$

where

$$f_{2n}(\theta,\theta_R)=f_{2n}^{b_0}(\theta,\theta_R)-if_{2n}^{\infty}(b,\theta_R)\ . \tag{13}$$

This is the final expression for the Glauber-eikonal scattering amplitude for a fixed orientation of the molecular axis $\mathbf{R}$.

The above amplitude, in the adiabatic approximation,[7] yields for the state-to-state DCS [Eq. (14)] and average elastic DCS [Eq. (16)]

$$I(j\to j',\theta)=\frac{k_i^2(2j'+1)}{16}\sum_{m=-j}^{j}\sum_{m'=-j'}^{j'}\lambda_n^2\left|\left[\frac{(j-|m|)!}{(j+|m|)!}\frac{(j'-|m'|)!}{(j'+|m'|)!}\right]^{1/2}\langle f_{2n}(\theta,\theta_R)\rangle\right|^2 , \tag{14}$$

with

$$\langle f_{2n}(\theta,\theta_R)\rangle=\int P_{j'}^{|m'|}(\cos\theta_R)f_{2n}(\theta,\theta_R)\times P_j^{|m|}(\cos\theta_R)\sin\theta_R\,d\theta_R\ , \tag{15}$$

$$2n=|m-m'|\ ,$$

$$\lambda_n=\begin{cases}2 & \text{for } n=0\\ 1 & \text{for } n\neq 0\ ,\end{cases}$$

$$\langle I(\theta)\rangle=\frac{k_i^2}{4}\sum_{n=0}\lambda_n\int|f_{2n}(\theta,\theta_R)|^2\sin\theta_R\,d\theta_R\ . \tag{16}$$

Total cross sections $\sigma(j\to j')$ for the transition $j\to j'$ or the average total elastic cross sections $\langle\sigma\rangle$ are calculated using Eq. (14) or Eq. (16) in

$$\sigma=2\pi\int_0^{\pi} I\sin\theta\,d\theta\ . \tag{17}$$

Finally, in order to show the advantage gained by dividing the b-integration range in Eq. (1) into two zones at $b=b_0$, we consider the z integration in Eq. (9). For sufficiently large values of r, say $r\geq r_0$, $V^{2l}(r)$ can be replaced by its asymptotic expression

$$V^{2l}(r\geq r_0)=-\frac{Q_{2l}}{r^{2l+1}}-\frac{\alpha_{2l}}{2r^4}\ , \tag{18}$$

where $Q_{2l}(l\geq 1)$ is the electric moment and α_{2l} $(l=0,1)$ is the dipole polarizability of the molecule. We take $b_0=r_0$ so that Eq. (9) becomes

$$I^{2l,2n}(b)=I^{2l,2n}(b,r<r_0)+I^{2l,2n}(b,r\geq r_0)\ , \tag{19}$$

where

$$I^{2l,2n}(b,r<r_0)=\frac{2}{v_i}\int_0^{z_0} V^{2l}(r<r_0)P_{2l}^{|2n|}(\cos\theta_r)dz\ , \tag{20}$$

$$I^{2l,2n}(b,r\geq r_0)=\frac{2}{v_i}\int_{z_{0,0}}^{\infty} V^{2l}(r\geq r_0)P_{2l}^{|2n|}(\cos\theta_r)dz\ . \tag{21}$$

Thus, for $b<b_0$, $I^{2l,2n}(b)$ is given by Eq. (19) in which the second term [Eq. (21)] with the nonzero lower limit z_0, defined by the relation $r_0^2=b^2+z_0^2$, is to be considered. For $b\geq b_0$, only the second term in Eq. (19) with the lower limit being zero in Eq. (21) becomes effective. Equation (21) can be further simplified using the asymptotic expression (18)

$$I^{2l,2n}(b,r\geq r_0)=-\frac{2}{v_i}\frac{Q_{2l}}{b^{2l}}\int_{\mu_{0,0}}^{1}P_{2l}^{|2n|}(\mu)(1-\mu^2)^{l-1}d\mu-\frac{1}{v_i}\frac{\alpha_{2l}}{b^3}\int_{\mu_{0,0}}^{1}P_{2l}^{|2n|}(\mu)(1-\mu^2)^{1/2}d\mu\ , \tag{22}$$

where $\mu_0=z_0/(b^2+z_0^2)^{1/2}$. Equation (20) is to be evaluated numerically. But the integral (22) can be obtained analytically. As a result, computation of $f^{\infty}(\theta,\hat{\mathbf{R}})$ [Eq. (11)] for $b\geq b_0$ reduces to the evaluation of the integral

$$\int_{qb_0}^{\infty}\frac{J_1(qb)}{qb}d(qb)$$

which can be readily performed by using a polynomial expansion for $J_1(x)/x$ following Roy and Sil.[22] Furthermore, in this case, analytic evaluation of $\langle f_{2n}^{\infty}(\theta,\theta_R)\rangle$ in Eq. (15) becomes straightforward.

III. EFFECTIVE ELECTRON-MOLECULE POTENTIAL

A. A brief survey

In the effective potential approach electron scattering by molecular targets is described by the potential $V(\mathbf{r},\hat{\mathbf{R}})$ which consists of three parts (we suppress $\hat{\mathbf{R}}$ in the argument for brevity),

$$V(\mathbf{r})=V_s(\mathbf{r})+V_{\rm ex}(\mathbf{r})+V_{\rm co}(\mathbf{r})\ . \tag{23}$$

The static potential $V_s(\mathbf{r})$ represents the effects of interaction between the incident electron and the unperturbed ground electronic charge distribution. $V_{\rm ex}(\mathbf{r})$ is the effective local exchange potential which takes into account the nonlocal electron-exchange effects due to the exclusion

principle, and $V_{co}(\mathbf{r})$ represents the correlation effects resulting from the interaction of the incident electron with the distorted molecular target. Much of the difficulties encountered in the theoretical study of electron scattering is due to the last two effects.

For exchange potential $V_{ex}(\mathbf{r})$, two approximations are widely used in electron scattering problems: Hara's version[17] of the free-electron-gas exchange (HFEG) approximation and the semiclassical exchange (SCE) approximation of Riley and Truhlar.[23] In the present paper we have considered the first approximation. The free-electron-gas (FEG) exchange potential[24] for a bound electron is given by

$$V_{ex}(\mathbf{r})=-\frac{2}{\pi}K_F F[\eta(\mathbf{r})] , \tag{23'}$$

where

$$F[\eta]=\frac{1}{2}+\frac{1-\eta^2}{4\eta}\ln\left|\frac{1+\eta}{1-\eta}\right| \tag{24}$$

with

$$\eta(\mathbf{r})=K(\mathbf{r})/K_F(\mathbf{r}) \tag{25}$$

defined in terms of local momentum $K(\mathbf{r})$ of the electron and the local Fermi momentum

$$K_F(\mathbf{r})=[3\pi^2\rho(\mathbf{r})]^{1/3} , \tag{26}$$

$\rho(\mathbf{r})$ being the local electron density. For scattering problems $\eta(\mathbf{r})>1$ and assuming that the incident and molecular electrons are in the same potential field Hara[17] obtained for $K(\mathbf{r})$,

$$K(\mathbf{r})^2=K_F(\mathbf{r})^2+2I+k_i^2 , \tag{27}$$

where I is the ionization potential of the target. The HFEG potential defined by Eqs. (23)—(27) is known to underestimate exchange effects and some authors,[25] to compensate for this, treat the ionization potential I as a parameter. This potential is known as tuned free-electron-gas (TFEG) exchange potential. Equation (27) shows that the HFEG potential asymptotically yields $\frac{1}{2}k_i^2+I$ for the kinetic energy of the incident electron, instead of $\frac{1}{2}k_i^2$. Thus an asymptotically adjusted potential (AAFEG) is sometimes devised,[23] by setting $I=0$, to reproduce correctly the incident energy at large r.

Theoretically, it is quite difficult to take into account properly the correlation effects $V_{co}(\mathbf{r})$. However, for large r, the long-range (LR) part of the correlation potential results in the dipole polarization potential $V_p(\mathbf{r})$ which, for molecular targets, can be written as

$$V_{co}^{LR}(\mathbf{r})\equiv V_p(\mathbf{r})=V_p^0(r)+V_p^2(r)P_2(\hat{\mathbf{r}}\cdot\hat{\mathbf{R}}) , \tag{28}$$

where V_p^0 and V_p^2 are given by the last term in Eq. (18). Small-r behavior of $V_p(\mathbf{r})$ is not known accurately.[5] For simple molecules, a few calculations[26] are available,[27–29] but such a calculation for larger systems is prohibitively difficult. For this reason, usually a cutoff function[5,30] with an adjustable parameter is used together with (28). The cutoff parameter is determined either from a knowledge of molecular structure or by reproducing known theoretical results of more rigorous calculations, or an experimental feature such as resonance.

Recently, O'Connell and Lane[14] (OL) have suggested a method of obtaining a model potential for $V_{co}(\mathbf{r})$. This potential is a hybridization of local FEG correlation energies and the long-range polarization energies. It is free from any adjustable parameter, while easy to apply even for complex targets. OL have applied it successfully to electron scattering by noble gases. According to them the short-range (SR) part of the correlation potential $V_{co}(\mathbf{r})$ effective for small r is defined as

$$V_{co}^{SR}(\mathbf{r})=2\epsilon_{co}(\mathbf{r}) , \tag{29}$$

where $\epsilon_{co}(\mathbf{r})$ is the local FEG correlation energy[15,31]

$$\epsilon_{co}(\mathbf{r})=\begin{cases}0.0311\ln r_s-0.048+0.009r_s\ln r_s-0.018r_s , & r_s\le 0.7\\ -0.061\,55+0.018\,98\ln r_s , & 0.7<r_s<10\\ -0.438r_s^{-1}+1.325r_s^{-3/2}-1.47r_s^{-2}-0.4r_s^{-5/2} , & r_s\ge 10\end{cases} \tag{30}$$

with

$$r_s=[3/(4\pi\rho)]^{1/3} . \tag{31}$$

$V_{co}^{SR}(\mathbf{r})$ is aspherical for molecular targets and can be expanded in Legendre polynomials

$$V_{co}^{SR}(\mathbf{r})=V_{co}^0(r)+V_{co}^2(r)P_2(\hat{\mathbf{r}}\cdot\hat{\mathbf{R}}) . \tag{32}$$

Since the FEG approximation takes no account of long-range interaction caused by polarization of the target, expressions (28) and (29) are joined smoothly at the point r_c^v, where they first cross each other. We call this hybrid potential $V_{co\text{-}p}(\mathbf{r})$ to distinguish it from polarization potentials $V_p(\mathbf{r})$ described in the preceding paragraph.

Padial and Norcross[15] (PN) calculated $V_{co\text{-}p}(\mathbf{r})$ for a few molecules, including polars. But they redefined Eq. (29) following Kohn and Sham:[32]

$$V_{co}^{SR}(\mathbf{r})=\frac{\partial}{\partial\rho}[\rho\epsilon_{co}(\mathbf{r})] . \tag{33}$$

They found that the values of $V_{co\text{-}p}^0(r=r_c^0)$ are independent of the target molecule used, an observation first pointed out by OL for noble gases. Furthermore, application to e-H_2 and e-N_2 scattering at low energies have revealed that $V_{co\text{-}p}$ obtained by using Eqs. (33) and (28) is somewhat stronger and PN have suggested that an *ad hoc* reduction of it could yield improved results. They have cited a better calculation of correlation energy by Perdew and Zunger[33] (PZ) which yields the following form of $V_{co}^{SR}(\mathbf{r})$:

$$V_{co}^{SR}(\mathbf{r})=\begin{cases}0.0311\ln r_s-0.0584+0.001\,33r_s\ln r_s-0.0084r_s, & r_s<1\\ \dfrac{\gamma(1+\frac{7}{6}\beta_1 r_s^{1/2}+\frac{4}{3}\beta_2 r_s)}{(1+\beta_1 r_s^{1/2}+\beta_2 r_s)^2}, & r_s>1\end{cases} \tag{34}$$

where $\gamma=-0.1423$, $\beta_1=1.0529$, and $\beta_2=0.3334$. Since this correlation potential is weaker than that given by Eq. (33) by about 15% for $r_s<10$, PN have recommended the use of it in computing $V_{co\text{-}p}(\mathbf{r})$ following O'Connell and Lane.[14]

B. Model potentials for e-H_2 scattering

For e-H_2 scattering, we have devised two groups of potentials, groups A and B, which differ mainly in the method of incorporating $V_{co}(\mathbf{r})$, the effects of correlations resulting from the interaction of the incident electron with the distorted target. For $V_{co}(\mathbf{r})$, we have used $V_{co\text{-}p}(\mathbf{r})$ in the group-A potentials, while $V_p(\mathbf{r})$ is used in group-B potentials. For $V_{co\text{-}p}(\mathbf{r})$, we have used the small-r form of $V_{co}(\mathbf{r})$ of PZ, Eq. (34). For comparison, $V_{co\text{-}p}(\mathbf{r})$ is also generated by using the other two forms of OL, Eq. (29), and PN, Eq. (33). Polarization potential for the e-H_2 system has been calculated by Lane and Henry,[27(a)] Truhlar *et al.*,[26] and Gibson and Morrison.[28] In the present paper we have used for $V_p(\mathbf{r})$ the analytic expressions, as given by Henry and Lane[16] (HL), which reproduce quite accurately the Lane and Henry[27(a)] polarization potential obtained by using the polarized orbital method.

For each of the groups of potential two types of FEG exchange potentials are considered: (a) the HFEG potential in which experimentally determined value, 0.564 a.u., is used for the ionization potential I, denoted by H, and (b) the TFEG potential for which I is treated as a parameter, denoted by $H(I_p)$. We have taken $I_p=0.071$ a.u. which is obtained by Morrison and Collins[25] by reproducing exact static exchange cross sections at $k_i^2=0.08$ a.u. Finally, a particular potential model is defined by mentioning the group and $V_{co}(\mathbf{r})$ and $V_{ex}(\mathbf{r})$ used, in the form (group)-$V_{co}(\mathbf{r})$-$V_{ex}(\mathbf{r})$. In Table I we have summarized the potential models used in the present paper. For each potential model the same static potential $V_s(\mathbf{r})$ is used.

We have used the Fraga and Ransil[19] H_2 wave function for equilibrium internuclear separation of $1.402a_0$ to calculate charge density $\rho(\mathbf{r})$. This charge density is then utilized to calculate $V_s(\mathbf{r})$ and different $V_{co\text{-}p}(\mathbf{r})$ and $V_{ex}(\mathbf{r})$ potentials. Calculations are performed using standard computer codes.[34] In Table II different characteristic data for e-H_2 potential are given. The Fraga-Ransil wave function was used earlier by different workers.[15,25] It yields a quadrupole moment of $0.48ea_0^2$ which is akin to the highly accurate theoretical[35] value of $0.484ea_0^2$ as well as to the experimentally[36] obtained value of $(0.474\pm0.34)ea_0^2$. For static and exchange potentials, expansion terms for $\nu=0$–6 are considered. For $V_{co\text{-}p}(\mathbf{r})$, terms other than $\nu=0$ and 2 are found to be negligible at small r compared to corresponding static potential terms. This is also observed by PN[15] for similar types of molecules ($D_{\infty h}$ symmetry).

TABLE I. Nomenclature of e-H_2 potential models.[a]

Group	$V_{co}(\mathbf{r})$ $V_{co\text{-}p}(\mathbf{r})$	$V_p(\mathbf{r})$	$V_{ex}(\mathbf{r})$	Model
A	PZ		HFEG	A-PZ-H
A	PZ		TFEG	A-PZ-$H(I_p)$
A	PZ		no	A-PZ-X[b]
A	OL		TFEG	A-OL-$H(I_p)$
A	PN		TFEG	A-PN-$H(I_p)$
B		HL	HFEG	B-HL-H
B		HL	TFEG	B-HL-$H(I_p)$
B		HL	no	B-HL-X

[a]Abbreviations used are explained in the text.
[b]X indicates that $V_{ex}(\mathbf{r})$ is neglected.

The different spherical parts (excluding exchange) of e-H_2 potential are shown in Fig. 1. The $V^0_{co\text{-}p}$ potential of OL is stronger than that of PN and PZ and the polarization potential V_p^0 of HL over the entire region $0\le r\le 7a_0$. In the region $0\le r\le r_c^0$, PZ potential is weaker than PN potential, but both of them appear to be a smoothed-out HL potential; these potentials are, however, stronger than the HL potential above $r=r_c^0$ and up to $r=7a_0$. Of the three $V_{co\text{-}p}$ potentials, PZ has the largest characteristic radius r_c^0 with the smallest value for $V^0_{co\text{-}p}(r_c^0)$.

IV. NUMERICAL PROCEDURE AND CONVERGENCE

Differential cross sections (14) and (16) are obtained numerically in two steps: first by performing z integration in Eq. (19) and then the b and θ_R integrations in relevant expressions (10′), (11′), (15), and (16). In the present calculations we set $b_0=r_0=10a_0$ (see the last paragraph of this section). For $b\le b_0$, the region $0\le b\le b_0$ is divided into 30 variable-step-size zones. Each of these zones is subdivided by using 8-point Gauss-Legendre quadrature. Using these values of b, z integration is performed numerically when $r\le r_0$ [Eq. (20)] and analytically when $r\ge r_0$ [Eq. (21)]. In the case of numerical integration, the integrated region $0\le z\le z_0$ is divided, depending on b, into a number of variable-step-size meshes, each mesh being evaluated by using 8-point Gauss-Legendre quadrature. Potential coefficients needed at Gaussian points within the region $0\le r\le r_0$ (V_s^{2l} and V_{ex}^{2l}) and $0\le r\le r_c^{2l}$ ($V^{2l}_{co\text{-}p}$) are obtained by spline-fitting these potentials calculated earlier at an interval of $r=0.05a_0$. Furthermore, excepting for V_{ex}^{2l}, Eq. (19) depends on energy through the factor $1/v_i$ and this is carefully exploited to reduce computer

TABLE II. Characteristic data for e-H_2 potential model in atomic units.

$V_{co\text{-}p}$[a]	r_c^0	r_c^2	$V^0_{co\text{-}p}(r_c^0)$	I	I_p[b]	Q_2[a]	α_0[c]	α_2[c]
OL	2.46	3.32	−0.071	0.564	0.071	0.48	5.179	1.202
PN	2.94	4.83	−0.035					
PZ	3.05	4.60	−0.030					

[a]Obtained by using Fraga-Ransil wave function (Ref. 19).
[b]Reference 25.
[c]Reference 35.

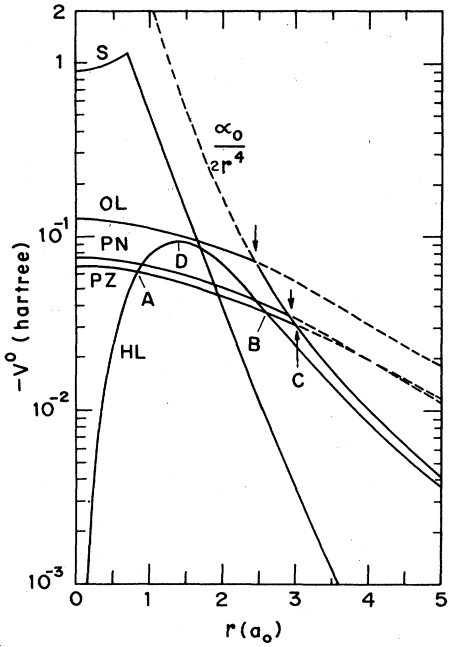

FIG. 1. Spherically symmetric part of e-H_2 potential: S, Fraga-Ransil static potential $V_s^0(r)$; OL, PN, and PZ, correlation-polarization potentials $V_{co\text{-}p}^0(r)$ of O'Connell and Lane, of Padial and Norcross, and of Perdew and Zunger, respectively (above the region $r=r_c^0$, marked by arrows, these potentials are represented by long-range polarization potential $-\alpha_0/2r^4$); HL, polarization potential $V_p^0(r)$ of Henry and Lane (Ref. 16).

time while computing cross sections at different energies. Finally, integration over molecular angles θ_R is performed using 12-point Gauss-Legendre quadrature. In this case, however, the dependence of cross sections on even functions of θ_R is properly utilized. For $b \geq b_0$, the significant simplification achieved in computing the amplitude $f^{\infty}(\theta,\hat{\mathbf{R}})$, and hence the cross sections, is described earlier in Sec. II. Integrated cross sections (17) are obtained by using the Simpson's rule.

Equation (14) shows that the highest-order term in $f_{2n}(\theta,\theta_R)$ [Eq. (13)] determined by the maximum value of n that contributes to $I(j\to j',\theta)$ depends upon the rotational states j and j'. It is found that $f_{2n}^{b_0}(\theta,\theta_R)$ [Eq. (10′)], for a particular value of n, converges when terms up to $p,q=4$ are considered. The series in (16) converges rapidly with increasing n and truncation at $n=2$ gives well-convergent results.

The accuracy of computed cross sections in the one-center approximation [Eq. (4)] depends upon the convergence of different cross sections with respect to increasing expansion terms ν. The convergence of different cross sections at 60 and 200 eV achieved in the present calculations with a limited number of terms ($\nu_{\max}=6$) of the potential model A-PZ-$H(I_p)$ is shown in Table III. It is found that integrated cross sections $\langle\sigma\rangle$ and the DCS $\langle I(\theta)\rangle$ at small and intermediate angles are well converged. Inclusion of potential terms with $\nu>2$ greatly influences the large-angle scattering at 200 eV.

For a particular value of b the phase term $\chi(b,\hat{\mathbf{R}})$ [Eqs. (7)—(9)] depends on the strength of the electron-molecule potential in the region $b \leq r \leq \infty$ and on the incident energy. When b equals four to five times the internuclear distance R, the strength of the potential in this region becomes such that, for most targets, $I^{2l,2n}(b) \ll 1$, even for incident energy as low as a few electron volts. This value of b is usually less than r_0 at and above which the asymptotic expression (18) becomes valid. Thus the choice of $b_0=r_0$ meets the essential requirement for b_0, e.g., $\chi(b,\hat{\mathbf{R}}) \ll 1$. In the present case, the expression (18) is exact at $r \geq r_0=10a_0$ for static and correlation-polarization potentials; for HL polarization potential we have used, to be precise, the expression $-\alpha_{2l}/2(r^2\pm a_{2l}^2)^2$, where the upper sign corresponds to $l=0$ and a_{2l} are constants.[16] At $b=10a_0$ we find that $I^{2l,2n}(b)\sim 10^{-3}$ with $b_0=r_0=10a_0$ for incident energy 5 eV (note that the major contribution to $I^{2l,2n}$ comes from the spherical part of the polarization potential). To test how sensitive the present calculations are to this choice of b_0 we have computed relevant cross sections with two different values of b_0, namely, $8a_0$ and $12a_0$. In both the cases, cross sections obtained are found to be identical with those for $b_0=10a_0$ [potential model A-PZ-$H(I_p)$ results for $b_0=12a_0$ are shown in Table III].

V. RESULTS AND DISCUSSIONS

In the present paper we have calculated the state-to-state DCS $I(j\to j',\theta)$ and integrated cross sections

TABLE III. Convergence of integrated cross sections $\langle\sigma\rangle$ (10^{-20} m^2) and DCS $\langle I(\theta)\rangle$ (10^{-20} m^2/sr) for e-H_2 scattering using the model A-PZ-$H(I_p)$.

Energy (eV)	$\nu\leq$	$\langle\sigma\rangle$	$\langle I(\theta)\rangle$ 5°	50°	150°	180°
60	2	1.415	2.980	1.040^{-1} [a]	7.050^{-3}	6.357^{-3}
	4	1.380	2.948	9.960^{-2}	7.114^{-3}	6.490^{-3}
	6	1.366	2.938	9.785^{-2}	6.846^{-3}	6.246^{-3}
	6[b]	1.366	2.938	9.786^{-2}	6.848^{-3}	6.247^{-3}
200	2	4.183^{-1}	2.078	1.329^{-2}	1.527^{-4}	8.795^{-5}
	4	4.197^{-1}	2.067	1.324^{-2}	6.399^{-4}	5.330^{-4}
	6	4.180^{-1}	2.063	1.309^{-2}	6.862^{-4}	5.843^{-4}
	6[b]	4.180^{-1}	2.063	1.310^{-2}	6.858^{-4}	5.839^{-4}

[a] x^n stands for $x\times 10^n$.

[b] Calculated with $b_0=12a_0$ and $r_0=10a_0$.

$\sigma(j\rightarrow j')$ for the pure elastic processes $j=0\rightarrow j'=0$ and $j=1\rightarrow j'=1$ and rotational-excitation processes $j=0\rightarrow j'=2$ and $j=1\rightarrow j'=3$. We have also computed the orientationally averaged elastic DCS $\langle I(\theta)\rangle$ and integrated cross sections $\langle\sigma\rangle$ as well as momentum-transfer cross sections $\langle\sigma_m\rangle$. Calculations are made using the potential models A-PZ-H and B-HL-H at 20—100 eV, A-PZ-$H(I_p)$ and B-HL-$H(I_p)$ at 20—200 eV, and A-PZ-X and B-HL-X at 20—400 eV. Test calculations are performed at energies 40 and 100 eV with the models A-PN-$H(I_p)$ and A-OL-$H(I_p)$.

A. Average elastic differential scattering cross sections

1. Comparison with experiments

Recently, a number of measurements of elastic DCS for e-H_2 scattering has appeared in the literature. These measurements do not discriminate rotational and vibrational excitation. We have considered only those measurements[37—40] which are recommended by Trajmar *et al.*[41] in a recent review article. Measurements of Wingerden *et al.*[39] at 100—2000 eV and 5—55°, of Srivastava *et al.*[37] (subsequently renormalized[41]) at 3—75 eV and 20—135°, and of Shyn and Sharp[40] at 2—200 eV and 6—156° are absolute, while those of Fink *et al.*[38] at 100—1000 eV and 3—130° are relative. The data as reported by the authors themselves are used for comparison.

We first concentrate on the models A-PZ-$H(I_p)$ and B-HL-$H(I_p)$. Average elastic DCS for these models are presented in Tables IV and V and are compared with experiments in Figs. 2—8. We find that both the models, in general, give excellent agreement with the experimental data of Shyn and Sharp at 150, 100, and 60 eV, but systematically underestimate these between 40—20 eV. The data of Srivastava *et al.*[37,41] are in excellent agreement with our results between 60—30 eV, and are closer than those of Shyn and Sharp to our results at 20 eV. At 75 eV, the only available experimental data are those reported by Srivastava *et al.* and the present cross sections overestimate these throughout the scattering angles. At 200 eV, measurements of Shyn and Sharp are in good agreement at small scattering angles, but increase systematically with increasing scattering angles. Considering the calculations with the models A-PZ-X and B-HL-X at 300 and 400 eV, the measurements of Fink *et al.* at 200 and 400 eV and those of Wingerden *et al.* at 100—400 eV are well reproduced. Only the large-angle measurements at 100 eV by Fink *et al.* are somewhat higher.

A detailed comparison of $\langle I(\theta)\rangle$ curves presented in Figs. 2—8 shows that the replacement of HL polarization potential V_p by PZ correlation-polarization potential $V_{co\text{-}p}$ modifies the angular dependence of $\langle I(\theta)\rangle$ at 30—400 eV. $\langle I(\theta)\rangle$ involving these potentials cross each other at a certain angle θ which decreases with increasing energy. Between 0° and θ, A-PZ-$H(I_p)$ cross sections are smaller; above θ and over a comparatively smaller angular region these are higher, and then become identical with B-HL-$H(I_p)$ cross sections. Interestingly all measurements[37—40] rather favor this augmentation in the angular dependence of $\langle I(\theta)\rangle$ arising from the replacement of HL V_p by PZ $V_{co\text{-}p}$.

To summarize, given the dispersion in the experimental data of different independent measurements, the theory

TABLE IV. Average elastic differential scattering cross sections $\langle I(\theta)\rangle$ (in 10^{-20} m^2/sr) for e-H_2 potential model A-PZ-$H(I_p)$.

	E (eV)							
θ (deg)	20	30	40	60	75	100	150	200
0	3.989	4.165	4.245	4.298	4.306	4.302	4.281	4.262
5	3.213	3.196	3.122	2.938	2.806	2.610	2.299	2.063
10	2.568	2.425	2.264	1.969	1.784	1.534	1.182	9.463^{-1}
15	2.036	1.822	1.622	1.299	1.115	8.851^{-1}	5.982^{-1}	4.319^{-1}
20	1.604	1.358	1.152	8.503^{-1}	6.928^{-1}	5.115^{-1}	3.111^{-1}	2.104^{-1}
25	1.257	1.008	8.162^{-1}	5.583^{-1}	4.351^{-1}	3.037^{-1}	1.735^{-1}	1.147^{-1}
30	9.822^{-1}[a]	7.473^{-1}	5.799^{-1}	3.721^{-1}	2.805^{-1}	1.890^{-1}	1.054^{-1}	6.905^{-2}
35	7.670^{-1}	5.562^{-1}	4.161^{-1}	2.543^{-1}	1.877^{-1}	1.244^{-1}	6.846^{-2}	4.732^{-2}
40	6.004^{-1}	4.175^{-1}	3.033^{-1}	1.793^{-1}	1.309^{-1}	8.600^{-2}	4.611^{-2}	2.816^{-2}
50	3.747^{-1}	2.451^{-1}	1.715^{-1}	9.785^{-2}	7.037^{-2}	4.482^{-2}	2.197^{-2}	1.309^{-2}
60	2.437^{-1}	1.538^{-1}	1.055^{-1}	5.847^{-2}	4.095^{-2}	2.480^{-2}	1.211^{-2}	7.982^{-3}
70	1.668^{-1}	1.029^{-1}	6.924^{-2}	3.689^{-2}	2.508^{-2}	1.504^{-2}	8.138^{-3}	5.553^{-3}
80	1.202^{-1}	7.238^{-1}	4.767^{-2}	2.444^{-2}	1.655^{-2}	1.042^{-2}	6.029^{-3}	3.988^{-3}
90	9.032^{-2}	5.305^{-2}	3.419^{-2}	1.729^{-2}	1.202^{-2}	8.004^{-3}	4.624^{-3}	2.895^{-3}
100	7.044^{-2}	4.033^{-2}	2.561^{-2}	1.318^{-2}	9.495^{-3}	6.482^{-3}	3.619^{-3}	2.105^{-3}
110	5.673^{-2}	3.180^{-2}	2.011^{-2}	1.073^{-2}	7.916^{-3}	5.413^{-3}	2.875^{-3}	1.548^{-3}
120	4.710^{-2}	2.604^{-2}	1.657^{-2}	9.163^{-3}	6.835^{-3}	4.631^{-3}	2.317^{-3}	1.176^{-3}
130	4.029^{-2}	2.214^{-2}	1.426^{-2}	8.104^{-3}	6.059^{-3}	4.049^{-3}	1.905^{-3}	9.362^{-4}
140	3.551^{-2}	1.951^{-2}	1.273^{-2}	7.362^{-3}	5.497^{-3}	3.618^{-3}	1.611^{-3}	7.833^{-4}
150	3.223^{-2}	1.776^{-2}	1.171^{-2}	6.846^{-3}	5.098^{-3}	3.306^{-3}	1.410^{-3}	6.863^{-4}
160	3.009^{-2}	1.665^{-2}	1.107^{-2}	6.504^{-3}	4.830^{-3}	3.094^{-3}	1.282^{-3}	6.268^{-4}
170	2.889^{-2}	1.603^{-2}	1.071^{-2}	6.309^{-3}	4.676^{-3}	2.971^{-3}	1.211^{-3}	5.945^{-4}
180	2.851^{-2}	1.583^{-2}	1.059^{-2}	6.246^{-3}	4.626^{-3}	2.931^{-3}	1.188^{-3}	5.843^{-4}

[a] x^n stands for $x\times 10^n$.

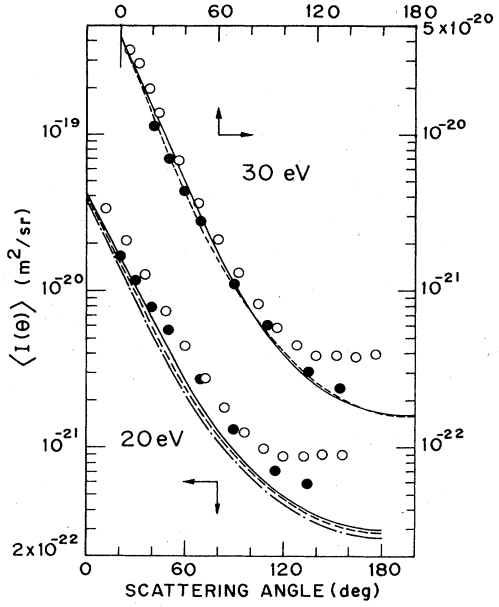

FIG. 2. Average elastic differential scattering cross sections at 20 and 30 eV as a function of scattering angle. Experimental: ●, Srivastava *et al.* (revised, Ref. 41); ○, Shyn and Sharp (Ref. 40). Theoretical: ——, potential model B-HL-$H(I_p)$; — — —, potential model A-PZ-$H(I_p)$; —·—·—·, potential model A-PZ-H. (Arrows indicate which scales apply.)

predicts the experimental data remarkably well, both in magnitude and shape, at 30—400 eV. The agreement between the theory and experiment is better at small and intermediate scattering angles. The deviation is prominent at large angles and it increases with decreasing energy. Models A-PZ-$H(I_p)$ (20—200 eV) and A-PZ-X (300 and 400 eV) give better fit to experiment than the corresponding B models.

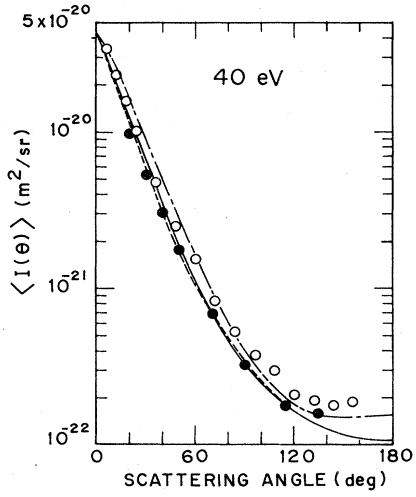

FIG. 3. Average elastic differential scattering cross sections at 40 eV. Experimental: ●, Srivastava *et al.* (revised, Ref. 41); ○, Shyn and Sharp (Ref. 40). Theoretical: ——, model B-HL-$H(I_p)$ and — — —, model A-PZ-$H(I_p)$ (present calculations); —·—, Truhlar and Brandt (model 3, thermally averaged, Ref. 56).

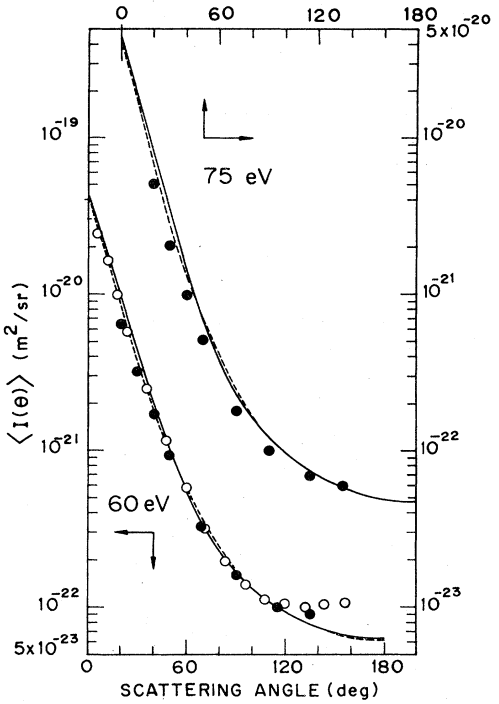

FIG. 4. Same as Fig. 2 but at 60 and 75 eV.

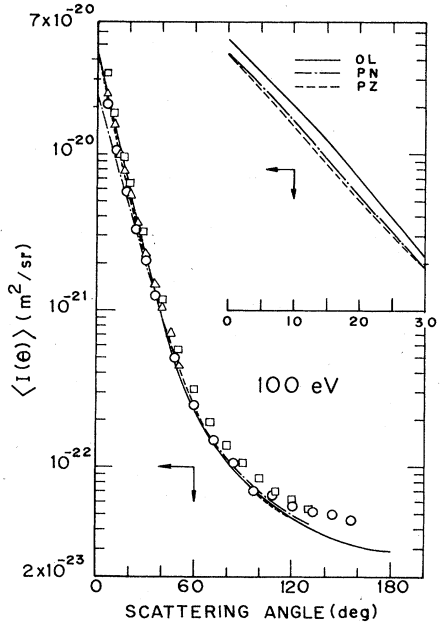

FIG. 5. Average elastic differential scattering cross sections at 100 eV. Lower panel: Experimental: ○, Shyn and Sharp (Ref. 40); □, Fink *et al.* (Ref. 38); △, van Wingerden *et al.* (Ref. 39). Theoretical: ——, model B-HL-$H(I_p)$ and — — —, model A-PZ-$H(I_p)$ (present calculations); —·—·—·, Khare and Shobha (Ref. 47). Upper panel: Comparison of small-angle cross sections for models A-OL-$H(I_p)$ (——), A-PN-$H(I_p)$ (—·—·—·), and A-PZ-$H(I_p)$ (— — —). (Arrows indicate which scales apply.)

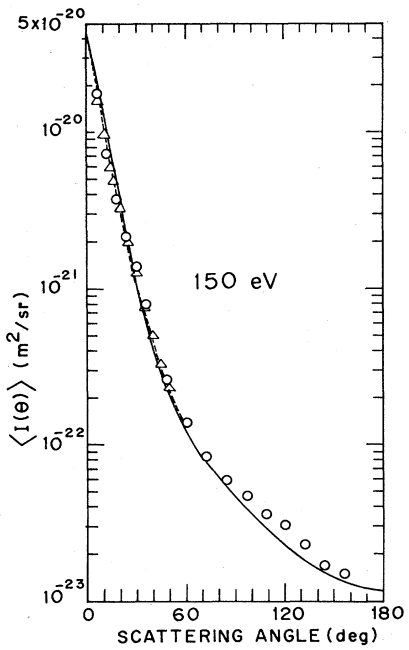

FIG. 6. Average elastic differential scattering cross sections at 150 eV. Experimental: ○, Shyn and Sharp (Ref. 40); △, van Wingerden *et al.* (Ref. 39). Theoretical: ——, model B-HL-$H(I_p)$ and — — —, model A-PZ-$H(I_p)$, present calculations.

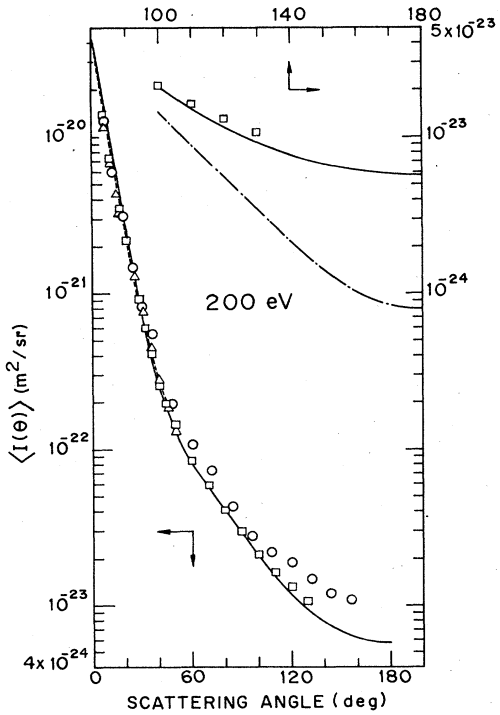

FIG. 7. Average elastic differential scattering cross sections at 200 eV. Lower panel: Experimental: ○, Shyn and Sharp (Ref. 40); □, Fink *et al.* (Ref. 38); △, van Wingerden *et al.* (Ref. 39). Theoretical: ——, model B-HL-$H(I_p)$ and — — —, model A-PZ-$H(I_p)$, present calculations. Upper panel: Comparison of large-angle scattering. Experimental: □, Fink *et al.* (Ref. 38). Theoretical: ——, model B-HL-$H(I_p)$, present calculations; —·—·—·, Bhattacharyya *et al.* (model B, Ref. 7). (Arrows indicate which scales apply.)

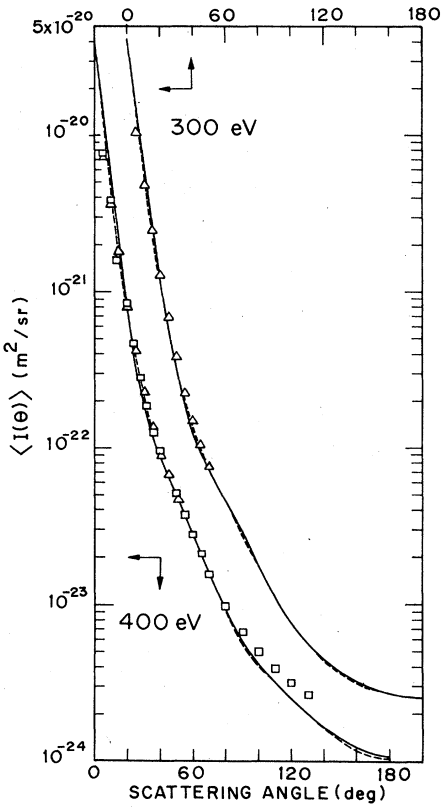

FIG. 8. Average elastic differential scattering cross sections at 300 and 400 eV. Experimental: □, Fink *et al.* (Ref. 38); △, van Wingerden *et al.* (Ref. 39). Theoretical: ——, model B-HL-X and — — —, model A-PZ-X, present calculations. (Arrows indicate which scales apply.)

We have presented the cross sections $\langle I(\theta)\rangle$ obtained by using the potential models A-PZ-H and B-HL-H in Tables VI and VII, respectively. The general features of $\langle I(\theta)\rangle$ curves for these models are similar to those for the pertinent models A-PZ-$H(I_p)$ and B-PZ-$H(I_p)$. This is illustrated in Fig. 2 for the models A-PZ-H and A-PZ-$H(I_p)$ and at incident energy 20 eV. The cross sections involving HFEG exchange potential are somewhat smaller in magnitude. The difference between the exchange models HFEG and TFEG reduces with increasing energy (Tables IV—VII).

In Fig. 5 we have compared $\langle I(\theta)\rangle$ at 100 eV and at scattering angles 0°—30° for the potential models involving different $V_{co\text{-}p}$ potentials. It is found that $\langle I(\theta)\rangle$ for the models A-PZ-$H(I_p)$ and A-PN-$H(I_p)$ are in reasonable agreement, but are considerably smaller in comparison with those of the model A-OL-$H(I_p)$.

2. *Comparison with other theoretical works*

The elastic scattering of electrons by hydrogen molecules has been extensively studied by using the Born approximation.[42–44] Attempts have been made to improve upon the Born approximation by including the effects of either electron exchange,[43,45] or polarization,[42,43] or both.[43,46–48] The exchange is usually treated by using the

TABLE V. Average elastic differential scattering cross sections $\langle I(\theta)\rangle$ (in 10^{-20} m^2/sr) for e-H_2 potential model B-HL-$H(I_p)$.

	E (eV)							
θ (deg)	20	30	40	60	75	100	150	200
0	3.949	4.156	4.253	4.325	4.340	4.342	4.329	4.314
5	3.196	3.210	3.154	2.992	2.870	2.686	2.392	2.168
10	2.583	2.476	2.337	2.067	1.894	1.657	1.313	1.076
15	2.084	1.906	1.726	1.421	1.241	1.010	7.079^{-1} [a]	5.226^{-1}
20	1.678	1.462	1.269	9.692^{-1}	8.055^{-1}	6.092^{-1}	3.779^{-1}	2.526^{-1}
25	1.347	1.117	9.273^{-1}	6.567^{-1}	5.197^{-1}	3.662^{-1}	2.031^{-1}	1.256^{-1}
30	1.077	8.493^{-1}	6.750^{-1}	4.441^{-1}	3.354^{-1}	2.215^{-1}	1.127^{-1}	6.667^{-2}
35	8.591^{-1}	6.445^{-1}	4.910^{-1}	3.012^{-1}	2.181^{-1}	1.368^{-1}	6.595^{-2}	3.872^{-2}
40	6.842^{-1}	4.892^{-1}	3.580^{-1}	2.061^{-1}	1.444^{-1}	8.734^{-2}	4.131^{-2}	2.472^{-2}
50	4.351^{-1}	2.849^{-1}	1.945^{-1}	1.020^{-1}	6.866^{-2}	4.052^{-2}	1.990^{-2}	1.276^{-2}
60	2.810^{-1}	1.715^{-1}	1.116^{-1}	5.575^{-2}	3.729^{-2}	2.249^{-2}	1.194^{-2}	8.099^{-3}
70	1.871^{-1}	1.088^{-1}	6.883^{-2}	3.397^{-2}	2.305^{-2}	1.450^{-2}	8.242^{-3}	5.647^{-3}
80	1.301^{-1}	7.333^{-2}	4.578^{-2}	2.283^{-2}	1.588^{-2}	1.043^{-2}	6.123^{-3}	4.045^{-3}
90	9.491^{-2}	5.249^{-2}	3.263^{-2}	1.666^{-2}	1.192^{-2}	8.085^{-3}	4.698^{-3}	2.907^{-3}
100	7.262^{-2}	3.966^{-2}	2.469^{-2}	1.301^{-2}	9.529^{-3}	6.565^{-3}	3.657^{-3}	2.101^{-3}
110	5.805^{-2}	3.142^{-2}	1.968^{-2}	1.071^{-2}	7.976^{-3}	5.492^{-3}	2.882^{-3}	1.547^{-3}
120	4.824^{-2}	2.595^{-2}	1.640^{-2}	9.187^{-3}	6.904^{-3}	4.696^{-3}	2.310^{-3}	1.177^{-3}
130	4.148^{-2}	2.224^{-2}	1.420^{-2}	8.142^{-3}	6.132^{-3}	4.095^{-3}	1.900^{-3}	9.363^{-4}
140	3.679^{-2}	1.970^{-2}	1.271^{-2}	7.410^{-3}	5.569^{-3}	3.646^{-3}	1.607^{-3}	7.814^{-4}
150	3.357^{-2}	1.798^{-2}	1.171^{-2}	6.900^{-3}	5.166^{-3}	3.320^{-3}	1.409^{-3}	6.832^{-4}
160	3.148^{-2}	1.688^{-2}	1.107^{-2}	6.563^{-3}	4.894^{-3}	3.100^{-3}	1.281^{-3}	6.235^{-4}
170	3.030^{-2}	1.626^{-2}	1.071^{-2}	6.370^{-3}	4.736^{-3}	2.973^{-3}	1.210^{-3}	5.913^{-4}
180	2.992^{-2}	1.606^{-2}	1.059^{-2}	6.307^{-3}	4.685^{-3}	2.931^{-3}	1.188^{-3}	5.812^{-4}

[a] x^n stands for $x \times 10^n$.

TABLE VI. Average elastic differential scattering cross sections $\langle I(\theta)\rangle$ (in 10^{-20} m^2/sr) for e-H_2 potential model A-PZ-H.

	E (eV)							
θ (deg)	20	30	40	60	75	100	300[a]	400[a]
0	3.730	3.976	4.101	4.209	4.239	4.257	4.064	4.088
5	2.977	3.028	2.998	2.864	2.752	2.576	1.616	1.401
10	2.358	2.282	2.161	1.911	1.744	1.510	6.007^{-1}	4.473^{-1}
15	1.855	1.703	1.540	1.256	1.086	8.691^{-1}	2.337^{-1}	1.602^{-1}
20	1.451	1.262	1.089	8.193^{-1}	6.732^{-1}	5.013^{-1}	1.075^{-1}	7.318^{-2}
25	1.130	9.322^{-1}	7.684^{-1}	5.366^{-1}	4.219^{-1}	2.973^{-1}	5.853^{-2}	3.855^{-2}
30	8.788^{-1} [b]	6.887^{-1}	5.444^{-1}	3.571^{-1}	2.718^{-1}	1.851^{-1}	3.410^{-2}	2.090^{-2}
35	6.839^{-1}	5.114^{-1}	3.901^{-1}	2.440^{-1}	1.820^{-1}	1.220^{-1}	2.024^{-2}	1.231^{-2}
40	5.342^{-1}	3.835^{-1}	2.843^{-1}	1.723^{-1}	1.271^{-1}	8.445^{-2}	1.284^{-2}	8.426^{-3}
50	3.334^{-1}	2.256^{-1}	1.614^{-1}	9.446^{-2}	6.868^{-2}	4.419^{-2}	7.035^{-3}	4.826^{-3}
60	2.178^{-1}	1.424^{-1}	9.987^{-2}	5.679^{-2}	4.016^{-2}	2.453^{-2}	4.482^{-3}	2.820^{-3}
70	1.501^{-1}	9.592^{-2}	6.605^{-2}	3.602^{-2}	2.469^{-2}	1.490^{-2}	2.882^{-3}	1.576^{-3}
80	1.088^{-1}	6.801^{-2}	4.578^{-2}	2.395^{-2}	1.632^{-2}	1.034^{-2}	1.813^{-3}	8.935^{-4}
90	8.239^{-2}	5.018^{-2}	3.300^{-2}	1.698^{-2}	1.188^{-2}	7.951^{-3}	1.142^{-3}	5.667^{-4}
100	6.462^{-2}	3.835^{-2}	2.480^{-2}	1.296^{-2}	9.932^{-3}	6.444^{-3}	7.668^{-4}	4.036^{-4}
110	5.228^{-2}	3.035^{-2}	1.951^{-2}	1.056^{-2}	7.839^{-3}	5.385^{-3}	5.602^{-4}	3.124^{-4}
120	4.356^{-2}	2.491^{-2}	1.609^{-2}	9.031^{-3}	6.774^{-3}	4.608^{-3}	4.410^{-4}	2.491^{-4}
130	3.736^{-2}	2.121^{-2}	1.386^{-2}	7.995^{-3}	6.009^{-3}	4.030^{-3}	3.687^{-4}	2.001^{-4}
140	3.299^{-2}	1.870^{-2}	1.238^{-2}	7.269^{-3}	5.454^{-3}	3.601^{-3}	3.214^{-4}	1.630^{-4}
150	2.997^{-2}	1.703^{-2}	1.140^{-2}	6.763^{-3}	5.059^{-3}	3.291^{-3}	2.889^{-4}	1.364^{-4}
160	2.800^{-2}	1.597^{-2}	1.077^{-2}	6.428^{-3}	4.794^{-3}	3.080^{-3}	2.670^{-4}	1.188^{-4}
170	2.690^{-2}	1.538^{-2}	1.043^{-2}	6.236^{-3}	4.642^{-3}	2.956^{-3}	2.542^{-4}	1.089^{-4}
180	2.654^{-2}	1.519^{-2}	1.032^{-2}	6.174^{-3}	4.592^{-3}	2.919^{-3}	2.500^{-4}	1.058^{-4}

[a] Without exchange (model A-PZ-X).

[b] x^n stands for $x \times 10^n$.

TABLE VII. Average elastic differential scattering cross sections (in 10^{-20} m^2/sr) for e-H_2 potential model B-HL-H.

	E(eV)							
θ (deg)	20	30	40	60	75	100	300[a]	400[a]
0	3.698	3.970	4.111	4.235	4.273	4.298	4.118	4.144
5	2.969	3.045	3.031	2.918	2.816	2.652	1.732	1.526
10	2.378	2.334	2.234	2.009	1.853	1.632	7.133^{-1}	5.439^{-1}
15	1.906	1.787	1.643	1.377	1.211	9.933^{-1}	2.883^{-1}	1.919^{-1}
20	1.526	1.365	1.203	9.364^{-1}	7.845^{-1}	5.982^{-1}	1.201^{-1}	7.350^{-2}
25	1.219	1.038	8.770^{-1}	6.334^{-1}	5.055^{-1}	3.592^{-1}	5.537^{-2}	3.354^{-2}
30	9.717^{-1}[b]	7.880^{-1}	6.374^{-1}	4.270^{-1}	3.261^{-1}	2.172^{-1}	2.952^{-2}	1.860^{-2}
35	7.735^{-1}	5.972^{-1}	4.633^{-1}	2.902^{-1}	2.121^{-1}	1.342^{-1}	1.812^{-2}	1.201^{-2}
40	6.56^{-1}	4.532^{-1}	3.378^{-1}	1.987^{-1}	1.405^{-1}	8.580^{-2}	1.244^{-2}	8.555^{-3}
50	3.921^{-1}	2.645^{-1}	1.839^{-1}	9.859^{-2}	6.698^{-2}	3.992^{-2}	7.160^{-3}	4.916^{-3}
60	2.544^{-1}	1.598^{-1}	1.059^{-1}	5.407^{-2}	3.651^{-2}	2.222^{-2}	4.564^{-3}	2.838^{-3}
70	1.703^{-1}	1.018^{-1}	6.559^{-2}	3.308^{-2}	2.265^{-2}	1.436^{-2}	2.901^{-3}	1.577^{-3}
80	1.189^{-1}	6.885^{-2}	4.378^{-2}	2.231^{-2}	1.566^{-2}	1.035^{-2}	1.812^{-3}	8.956^{-4}
90	8.694^{-2}	4.942^{-2}	3.131^{-2}	1.634^{-2}	1.177^{-2}	8.034^{-3}	1.145^{-3}	5.639^{-4}
100	6.659^{-2}	3.743^{-2}	2.377^{-2}	1.279^{-2}	9.429^{-3}	6.528^{-3}	7.661^{-4}	4.036^{-4}
110	5.323^{-2}	2.972^{-2}	1.900^{-2}	1.055^{-2}	7.902^{-3}	5.464^{-3}	5.574^{-4}	3.132^{-4}
120	4.422^{-2}	2.459^{-2}	1.588^{-2}	9.060^{-3}	6.844^{-3}	4.674^{-3}	4.402^{-4}	2.502^{-4}
130	3.802^{-2}	2.112^{-2}	1.377^{-2}	8.037^{-3}	6.082^{-3}	4.076^{-3}	3.692^{-4}	2.015^{-4}
140	3.372^{-2}	1.873^{-2}	1.235^{-2}	7.320^{-3}	5.526^{-3}	3.629^{-3}	3.223^{-4}	1.643^{-4}
150	3.077^{-2}	1.713^{-2}	1.139^{-2}	6.820^{-3}	5.128^{-3}	3.306^{-3}	2.898^{-4}	1.374^{-4}
160	2.886^{-2}	1.609^{-2}	1.077^{-2}	6.488^{-3}	4.858^{-3}	3.087^{-3}	2.680^{-4}	1.196^{-4}
170	2.778^{-2}	1.551^{-2}	1.043^{-2}	6.299^{-3}	4.702^{-3}	2.960^{-3}	2.553^{-4}	1.097^{-4}
180	2.743^{-2}	1.532^{-2}	1.032^{-2}	6.237^{-3}	4.651^{-3}	2.919^{-3}	2.511^{-4}	1.065^{-4}

[a]Without exchange (model B-HL-X).
[b]x^n stands for $x \times 10^n$.

Ochkur[47,48] or Ochkur-Rudge[43] approximation. Different forms of polarization potentials with adjustable parameters have been tried.[42,43,47,48] As a typical case, we consider the incident energy 100 eV. At this energy, the calculations Khare and Shobha[47] are compared in Fig. 5. It is found that the small-angle cross sections of these authors underestimate considerably the present cross sections as well as the experimental data, whereas the large-angle

TABLE VIII. State-to-state differential scattering cross sections (in 10^{-20} m^2/sr) for e-H_2 scattering at 40 eV.

	Model A-PZ-$H(I_p)$				Model B-HL-$H(I_p)$			
θ (deg)	$I(0\rightarrow0)$	$I(0\rightarrow2)$ ($\times10^{-3}$)	$I(1\rightarrow1)$	$I(1\rightarrow3)$ ($\times10^{-3}$)	$I(0\rightarrow0)$	$I(0\rightarrow2)$ ($\times10^{-3}$)	$I(1\rightarrow1)$	$I(1\rightarrow3)$ ($\times10^{-3}$)
0	4.239	5.700	4.241	3.463	4.246	6.207	4.249	3.764
5	3.115	6.416	3.118	3.935	3.147	6.946	3.150	4.267
10	2.256	7.027	2.259	4.307	2.329	7.738	2.332	4.749
15	1.614	7.512	1.617	4.594	1.718	8.558	1.721	5.235
20	1.144	7.881	1.148	4.815	1.259	9.375	1.263	5.724
25	8.078^{-1}[a]	8.169	8.111^{-1}	4.986	9.169^{-1}	1.015^{1}	9.210^{-1}	6.190
30	5.713^{-1}	8.410	5.746^{-1}	3.130	6.639^{-1}	1.085^{1}	6.683^{-1}	6.609
35	4.072^{-1}	8.635	4.107^{-1}	5.263	4.793^{-1}	1.144^{1}	4.839^{-1}	6.963
40	2.942^{-1}	8.858	2.978^{-1}	5.395	3.458^{-1}	1.191^{1}	3.506^{-1}	7.237
50	1.620^{-1}	9.290	1.658^{-2}	5.651	1.818^{-1}	1.241^{1}	1.868^{-1}	7.534
60	9.565^{-2}	9.630	9.950^{-2}	5.852	9.894^{-2}	1.244^{1}	1.039^{-1}	7.549
70	5.927^{-2}	9.787	6.318^{-2}	5.943	5.647^{-2}	1.215^{1}	6.133^{-2}	7.371
80	3.774^{-2}	9.743	4.164^{-2}	5.916	3.389^{-2}	1.168^{1}	3.856^{-2}	7.089
90	2.445^{-2}	9.545	2.827^{-2}	5.798	2.128^{-2}	1.113^{1}	2.573^{-2}	6.761
100	1.616^{-2}	9.255	1.986^{-2}	5.626	1.391^{-2}	1.056^{1}	1.814^{-2}	6.422
110	1.099^{-2}	8.924	1.456^{-2}	5.431	9.442^{-3}	1.001^{1}	1.345^{-2}	6.097
120	7.771^{-3}	8.590	1.121^{-2}	5.235	6.659^{-3}	9.506	1.046^{-2}	5.796
140	4.503^{-3}	7.993	7.701^{-3}	4.887	3.779^{-3}	8.673	7.248^{-3}	5.307
160	3.231^{-3}	7.593	6.268^{-3}	4.653	2.641^{-3}	8.150	5.901^{-3}	5.000
180	2.890^{-3}	7.454	5.871^{-3}	4.572	2.335^{-3}	7.973	5.524^{-3}	4.897

[a]x^n stands for $x \times 10^n$.

cross sections are comparable with the present ones. At small angles, a better agreement, however, is found to occur with the calculations of Truhlar and Rice (not shown).[46] At lower energies, Born approximation, even with the inclusion of polarization and exchange, give poor results.

Next to Born approximation, the Glauber approximation (and its different versions) is the alternate high-energy approximation which has been used[2,6,7,49–55] frequently for e-H_2 scattering. But most of the calculations reported so far, excepting those by our group,[2,6,7] essentially make use of the independent-atom approximation[49–53] (IAA) in which the effects of bonding is incorporated through an adjustable parameter. A notable exception is the Glauber calculation by LaGattuta[55] who has derived the scattering amplitude by considering a Gaussian basis for the electronic part of the target wave function. Their results at 40 and 100 eV are in poor agreement with the experimental data (see Figs. 1 and 2 of Ref. 55) as well as with the present calculations. The IAA[51–53] and modified Glauber[54] calculations, on the other hand, give good agreement throughout the scattering angles at and above 100 eV (not shown). Earlier calculations of Bhattacharyya *et al.*[7] (model B) show significant discrepancy in large-angle scattering compared to the present calculations with model B-HL-$H(I_p)$. This is illustrated in Fig. 7 for the incident energy 200 eV. Present calculations with potential terms $\nu \leq 2$ and $\nu \leq 6$ (Table III) indicate that this discrepancy arises mainly from the neglect of potential terms with $\nu > 2$ by Bhattacharyya *et al.*

In the energy region considered here only a few close-coupling calculations,[56–58] following either one-center[56,58] or two-center[57] techniques, have been reported so far. The most recent work of Staszewska *et al.*,[58] which is an improved version of the earlier work of Truhlar and Brandt,[56] takes into account the effects of electron excitation through an effective absorption potential. Their cross sections (model SEPa, without absorption) are in excellent agreement, both in magnitude and angular dependence, with those of ours at 100 eV, but are systematically higher in magnitude at 40 eV (not shown). At 40 eV, the cross sections (model 3, thermally averaged) obtained earlier by Truhlar and Brandt are also somewhat higher in magnitude (Fig. 3). Truhlar *et al.*[59] have also computed elastic cross sections at 20, 30, and 40 eV by employing the infinite-order sudden approximation. These cross sections considerably overestimate the present ones at all energies (not shown).

B. State-to-state differential scattering cross sections

At intermediate energies the only measurements of state-to-state differential scattering cross section available are those of Srivastava *et al.*[60] However, a few calculations at energies pertinent to the present investigation are made using the infinite-order sudden,[59] close-coupling,[56,58] and Glauber approximations.[6,7,55,61] For comparison we have considered the close-coupling cross sections of Truhlar and co-workers.[56,58]

In Table VIII different state-to-state cross sections at 40 eV obtained by using the models A-PZ-$H(I_p)$ and B-HL-$H(I_p)$ are presented. In Fig. 9 cross sections $I(1\rightarrow 1,\theta)$ and $I(1\rightarrow 3,\theta)$ at 40 eV for these models are compared with the corresponding experimental[60,41] and theoretical quantities.[56] It is found that $I(1\rightarrow 1,\theta)$ cross sections for either of the models are in excellent agreement, both in magnitude and shape, with those obtained experimentally. On the other hand, $I(1\rightarrow 3,\theta)$ cross sections for these models are about 2 to 4 times smaller and show completely opposite angular dependence. These cross sections for the model A-PZ-$H(I_p)$ are smaller at all scattering angles than those for model B-HL-$H(I_p)$. For both the processes, the close-coupling cross sections[56,58] are higher in magnitude, but show similar angular dependence in the case of the inelastic process.

Table VIII shows that pure elastic cross sections $I(j\rightarrow j,\theta)$ increase with the increase in the initial state J, but the corresponding inelastic cross sections $I(j\rightarrow j+2,\theta)$ decrease in such a way that the sum of the cross sections $I(j\rightarrow j,\theta)+I(j\rightarrow j+2,\theta)$ remains almost independent of j. Other characteristic features of the state-to-state cross sections, such as the energy dependence and the dominance of the inelastic cross sections

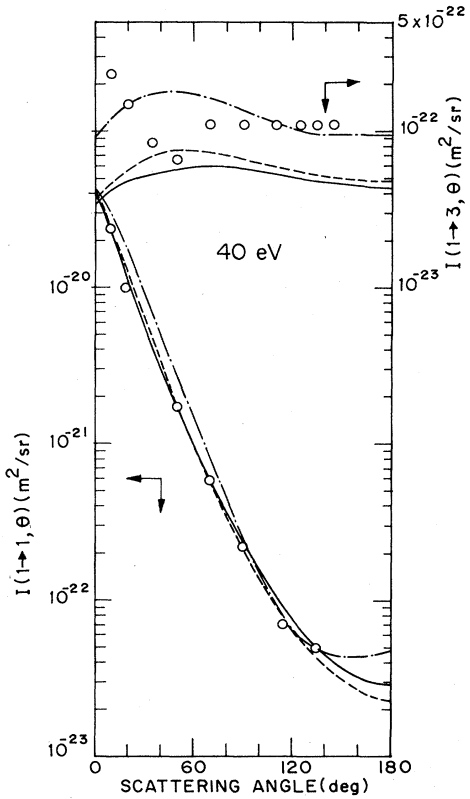

FIG. 9. Lower panel: Pure elastic differential scattering cross sections at 40 eV for the transition $j=1\rightarrow j'=1$. Upper panel: Pure rotational-excitation differential scattering cross sections at 40 eV for the transition $j=1\rightarrow j'=3$. Experimental: ○, Srivastava *et al.* (revised, Ref. 41). Theoretical: — — —, model B-HL-$H(I_p)$ and ——, model A-PZ-$H(I_p)$, present calculations; —·—·—·, Truhlar and Brandt (model 3, Ref. 56). (Arrows indicate which scales apply.)

TABLE IX. Integrated cross sections (10^{-20} m^2) for e-H_2 scattering obtained by using different group-A models: comparison with experimental and other theoretical results.

Energy (eV)	Model[a]	$\sigma(0\rightarrow0)$	$\sigma(0\rightarrow2)$ ($\times10^{-1}$)	$\sigma(1\rightarrow1)$	$\sigma(1\rightarrow3)$ ($\times10^{-1}$)	$\langle\sigma\rangle$	$\langle\sigma\rangle^b$	$\langle\sigma\rangle^c$	$\langle\sigma\rangle^d$
20	(i)	3.243	0.896	3.279	0.548	3.335	2.219	4.693[e]	4.15[f]
	(ii)	2.922	0.880	2.957	0.538	3.012			5.61[g]
				4.56[h]	7.09[h]			5.270[h]	
30	(i)	2.380	1.054	2.422	0.642	2.488	1.748	3.873[e]	2.30[f]
	(ii)	2.210	1.035	2.252	0.631	2.316		3.976[i]	3.36[g]
				3.04[h]	4.92[h]			3.54[h]	
40	(i)	1.849	1.118	1.894	0.681	1.964	1.442		1.70[f]
	(ii)	1.750	1.102	1.794	0.671	1.862			2.50[g]
	(iii)	1.924	1.123	1.969	0.684	2.039			
	(iv)	2.341	1.144	2.387	0.696	2.458			
				2.65[h]	3.79[h]			3.03[h]	
				3.503[j]	2.285[j]			3.732[j]	
60	(i)	1.253	1.095	1.297	0.668	1.366	1.068	1.960[e]	1.00[f]
	(ii)	1.210	1.084	1.254	0.661	1.321			1.27[g]
75	(i)	1.001	1.022	1.042	0.626	1.106	0.894		0.70[f]
	(ii)	0.975	1.014	1.016	0.623	1.080			
100	(i)	0.745	0.882	0.781	0.545	0.837	0.704	1.154[e]	0.77[g]
	(ii)	0.732	0.877	0.767	0.542	0.824		0.751[i]	0.89[k]
	(iii)	0.778	0.884	0.813	0.547	0.870		0.975[l]	
	(iv)	0.965	0.896	1.001	0.554	1.058		1.019[m]	
				1.338[j]	0.864[j]			1.427[j]	
150	(i)	0.490	0.647	0.515	0.410	0.559	0.493	0.471[i]	0.50[g]
								0.686[m]	0.52[k]
200	(i)	0.363	0.494	0.383	0.320	0.418	0.378	0.325[i]	0.39[g]
								0.515[m]	0.36[k]
300	b	0.221	0.322	0.234	0.214		0.258	0.210[i]	0.23[k]
400	b	0.167	0.245	0.177	0.164		0.196	0.159[i]	0.15[k]

[a]Models (i) A-PZ-$H(I_p)$, (ii) A-PZ-H, (iii) A-PN-$H(I_p)$, and (iv) A-OL-$H(I_p)$.
[b]Without exchange. Model A-PZ-X.
[c]Other theoretical results.
[d]Experimental.
[e]Reference 43 (*BOR/P*, Table IV; 20 eV, *B/P*, Table III).
[f]Reference 41 (renormalized data of Ref. 37).
[g]Reference 40.
[h]Reference 59.
[i]Reference 48 (model Q_c); for 30 eV, see Ref. 47.
[j]Reference 58 (model SEPa).
[k]Reference 39.
[l]Reference 50.
[m]Reference 42.

over the pure elastic cross sections at large angles, are identical with those observed earlier by Bhattacharyya *et al.*[7] When exchange effects are treated using the HFEG potential, instead of the TFEG potential, only the magnitudes of different cross sections are lowered.

C. Integrated and momentum-transfer cross sections

In Table IX integrated cross sections for different elastic and inelastic processes and for the average elastic scattering calculated by using different A models are compiled to compare their relative magnitudes. These quantities for the B models are given in Table X. Comparison with different experimental measurements[37–39] and with other theoretical calculations[42,43,47,48,50,58,59] are also made in Table IX. In general, we find that the cross sections $\langle\sigma\rangle$ are independent of the initial rotational state j of the molecule. Furthermore, these cross sections at 30–200 eV for the A models, A-PZ-$H(I_p)$ and A-PZ-H, and for the corresponding B models, B-HL-$H(I_p)$ and B-HL-H, are usually within the dispersion in the experimental data of different independent measurements. At 300 and 400 eV, where exchange effects are negligible, model A-PZ-X cross sections are closer to experimental data than model B-HL-X cross sections. At the lower part of the energy region, where exchange effects are prominent, the TFEG model is more effective than the HFEG model. In this region the model B cross sections, compared to corresponding model A cross sections, are more akin to experimental data. Nevertheless the nature of $\langle I(\theta)\rangle$ curves (Figs. 2–8) suggests that the potential models A-PZ-$H(I_p)$ and A-PZ-X (at 300 and 400 eV) give the best overall agree-

TABLE X. Integrated cross sections (10^{-20} m^2) for e-H_2 scattering obtained by using group-B models.

Energy (eV)	Model[a]	$\sigma(0\rightarrow0)$	$\sigma(0\rightarrow2)$ ($\times10^{-1}$)	$\sigma(1\rightarrow1)$	$\sigma(1\rightarrow3)$ ($\times10^{-1}$)	$\langle\sigma\rangle$	$\langle\sigma\rangle^b$
20	(i)	3.492	1.128	3.537	0.689	3.608	2.464
	(ii)	3.164	1.114	3.208	0.680	3.278	
30	(i)	2.567	1.287	2.619	0.784	2.699	1.932
	(ii)	2.392	1.267	2.442	0.772	2.521	
40	(i)	1.996	1.328	2.049	0.808	2.132	1.589
	(ii)	1.892	1.310	1.945	0.797	2.026	
60	(i)	1.355	1.253	1.405	0.764	1.483	1.173
	(ii)	1.310	1.241	1.360	0.757	1.437	
75	(i)	1.084	1.153	1.130	0.706	1.202	0.981
	(ii)	1.056	1.144	1.102	0.700	1.174	
100	(i)	0.808	0.982	0.847	0.606	0.910	0.771
	(ii)	0.794	0.977	0.833	0.603	0.896	
150	(i)	0.532	0.715	0.560	0.451	0.608	0.539
200	(i)	0.395	0.545	0.417	0.351	0.455	0.414
300	b	0.241	0.356	0.255	0.235		0.282
400	b	0.183	0.271	0.193	0.179		0.214

[a]Models (i) B-HL-$H(I_p)$ and (ii) B-HL-H.
[b]Without exchange. Model B-HL-X.

ment with the experimental measurements throughout the energy interval considered here. At 30—100 eV polarized Born (with exchange) calculations of Trajmar *et al.*[43] are about 1.56 to 1.4 times higher than the present calculations for the model A-PZ-$H(I_p)$. On the other hand, the calculations of Khare and Shobha[47] are about 1.6 times higher at 30 eV. The results of Gupta and Khare[48] are comparable only at 100 eV, but underestimate our results at still higher energies. The close-coupling cross sections (model SEPa) obtained by Staszewska *et al.*[58] overestimate the present ones at 40 eV by a factor of 1.9, while those at 100 eV by 1.7.

In Table XI momentum-transfer cross sections $\langle\sigma_m\rangle$ for different potential models are compared with those obtained experimentally[37,40] and theoretically[56,58,59] by different workers. It is observed that both the models A-PZ-$H(I_p)$ and B-HL-$H(I_p)$ give fairly good agreement with the measurements between 30—200 eV.

D. A few observations

1. Exchange

The exchange interaction modifies significantly the electron scattering cross sections at the low-energy region. In this energy region exact static exchange (ESE) calculations for simple molecules can be performed.[5,62,63] Thus a model exchange potential can be tested[25,64,65] by carefully comparing the predictions of this model (plus the static potential) with the accurate ESE calculations. For hydrogen molecules, Morrison and Collins[25] have made such a study by calculating the eigenphase sum and they have

TABLE XI. Momentum-transfer cross sections $\langle\sigma_m\rangle$ (10^{-20} m^2) for e-H_2 scattering.

Models	Energy (eV) 20	30	40	60	75	100	150	200
A-PZ-$H(I_p)$	1.164	0.724	0.498	0.284	0.207	0.137	0.073	0.046
A-PZ-H	1.056	0.679	0.475	0.276	0.203	0.135		
A-PZ-X	0.752	0.507	0.369	0.228	0.173	0.120	0.067	0.043
B-HL-$H(I_p)$	1.262	0.770	0.520	0.292	0.212	0.139	0.075	0.046
B-HL-H	1.149	0.721	0.497	0.285	0.208	0.138		
SCT[a]	1.73	0.801	0.515	0.268	0.167			
SS[b]	2.11	1.02	0.64	0.29		0.15	0.083	0.060
TPB[c]	1.55	0.747	0.441					
TB[d]			0.709					
SST[e]			1.026			0.212		

[a]Reference 41 (renormalized data of Ref. 37).
[b]Reference 40.
[c]Reference 59.
[d]Reference 56 (model 3).
[e]Reference 58 (model SEPa).

pointed out that the HFEG exchange model is to be properly tuned (TFEG) by adjusting the ionization potential to get an agreement with the ESE calculations. They have also found that the difference between the predictions of the two models decreases with the increasing energy.

At intermediate energies, no ESE cross sections, to our knowledge, are available. To test an exchange model we have to compare its predictions directly with the experimental cross sections $\langle\sigma\rangle$. In the present case, we observe that for the group A models with PZ $V_{co\text{-}p}$ potential the effect of exchange interaction is to increase the cross sections $\langle\sigma\rangle$ (see columns 7 and 8, Table IX) by about 36% at 20 eV to 17% at 100 eV for the model HFEG. The TFEG model, on the other hand, registers an increase of 50% (20 eV) to 19% (100 eV). Thus the two exchange models differ considerably at the lower part of the energy region considered here. The predictions of the two models gradually converge with increasing energy (this is also true for the group B models, as is evident from Table X). A comparison with the experimental data of Srivastava *et al.* and Shyn and Sharp (see columns 7 and 10, Table IX) suggests that TFEG cross sections are in better agreement compared to the HFEG ones. These observations indicate that HFEG exchange potential is weak even at intermediate energies and needs "tuning."

2. *Correlation polarization*

One of our major objectives of the present study is to investigate the usefulness of $V_{co\text{-}p}$ potential at intermediate energies. We have noted in Sec. IV A 1 that differential scattering cross sections $\langle I(\theta)\rangle$ involving PZ $V_{co\text{-}p}$ potential give better agreement with the experiment than those involving HL V_p potential. The region of PZ potential most effective in changing the angular dependence of $\langle I(\theta)\rangle$ when it replaces HL potential could be ascertained by examining the contributions of the spherical parts of these potentials to $\langle I(\theta)\rangle$. The relevant cross sections at 30 eV are presented in Fig. 10. In Fig. 1 the points A ($0.85a_0$), B ($2.5a_0$), and C ($3.05a_0$) of PZ $V^0_{co\text{-}p}$ and the minimum in HL V^0_p at D ($r=1.4a_0$) correspond, respectively, to the scattering angle 74°, 66°, 60°, and 70° shown in Fig. 10. Between the scattering angles 0°–74°, $V^0_s+V^0_{co\text{-}p}$ cross sections are smaller than $V^0_s+V^0_p$ ones; the situation reverses roughly above the scattering angle 74°. Apparently, $r=1.4a_0$–$2.5a_0$ is the most sensitive region of $V^0_{co\text{-}p}$ or V^0_p potentials. The effects of stronger HL V^0_p in this region more than compensate for the effects of stronger PZ $V^0_{co\text{-}p}$ in the region $r=2.5a_0$–$7a_0$. As a result $V^0_s+V^0_{co\text{-}p}$ cross sections become smaller than $V^0_s+V^0_p$ ones. Below $r=1.4a_0$ the nature of modulation of static potential V^0_s due to HL V^0_p and PZ $V^0_{co\text{-}p}$ changes $\langle I(\theta)\rangle$ roughly above the scattering angle 74° as shown in Fig. 10. When the nonspherical potential is switched on cross sections in this region are affected most.

Figure 1 shows that in the region $r=1.4a_0$–$2.5a_0$, PN $V^0_{co\text{-}p}$ lies between HL V^0_p and PZ $V^0_{co\text{-}p}$, whereas OL $V^0_{co\text{-}p}$ is even stronger than HL V^0_p potential. This is reflected in the relative magnitudes of $\langle I(\theta)\rangle$ (Fig. 5) and $\langle\sigma\rangle$ (Tables IX and X) computed at 40 and 100 eV by using these potentials.

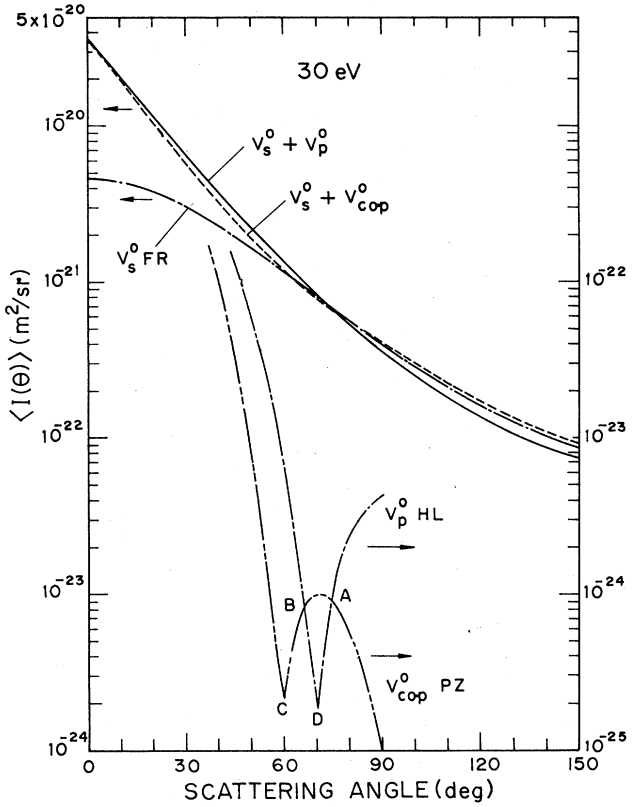

FIG. 10. Comparison of elastic differential scattering cross sections involving spherical part of Henry-Lane polarization ($V_s^0+V_p^0$) and Perdew-Zunger correlation-polarization ($V_s^0+V^0_{co\text{-}p}$) potentials. Elastic DCS for short-range Fraga-Ransil static potential V_s^0 and the long-range potentials HL V_p^0 and PZ $V^0_{co\text{-}p}$ alone are also shown. The scattering angles A, B, and C marked on the $V^0_{co\text{-}p}$ and D on the V_p^0 cross sections correspond to the positions in the pertinent potential shown in Fig. 1. (Arrows indicate which scales to apply.)

Rotationally inelastic cross sections depend upon the nonspherical parts of the electron-molecule potential. $I(1\rightarrow3,\theta)$ at 40 eV shown in Fig. 9 and $\sigma(j\rightarrow j+2)$ presented in Tables IX and X suggest that nonspherical PZ potential is much weaker than the nonspherical HL potential. Finally, we would like to point out one important aspect of the nonspherical polarization potential. All the known theoretical calculations[6,7,55,56,58,59] (including the present one), in which different static and polarization[66] potentials have been used by employing different quantum-mechanical approximations, fail[67] to reproduce the shape of experimental cross sections $I(1\rightarrow3,\theta)$. The only exception is the potential model A calculations of Bhattacharyya *et al.*[6,7] in which a Buckingham-type cutoff parameter is used[17] for V_p^2. This suggests that precise knowledge regarding the nonspherical polarization potential of hydrogen molecules is still lacking. However, more accurate experimental data are needed to confirm it.

VI. CONCLUSIONS

We have presented in the present paper an improved version of the Glauber-eikonal scattering amplitude origi-

nally developed by Bhattacharyya and Ghosh. We have used this amplitude to test a recently proposed, parameter-free model of correlation-polarization contribution to FEG electron-molecule potential by applying it to e-H_2 scattering at intermediate energies.

We observe that the correlation-polarization potential (PZ) employed is weaker than the Henry-Lane polarization potential and gives smaller average elastic and state-to-state integrated cross sections. For average elastic DCS and integrated cross sections, agreement between theory and experiment is better when calculations are made with the correlation-polarization potential. Correlation-polarization potential yields better cross sections when used in combination with the TFEG exchange potential [A-PZ-$H(I_p)$] than in combination with the HFEG exchange potential (A-PZ-H). This is because the HFEG model is weak for hydrogen molecules even at intermediate energies. For a two-electron system like H_2 the overall success of the correlation-polarization model is quite encouraging and further tests of the model on molecular targets possessing more electrons should be undertaken.

As for the present Glauber-eikonal amplitude, we find that inclusion of nonspherical potential terms with $\nu=4$ and 6 significantly improves the intermediate- and large-angle average elastic DCS; these cross sections at and above 100 eV become comparable with those obtained by using the polarized-Born approximation. At 30—100 eV the polarized-Born approximation gives poor results, but the present amplitude reproduces the small- and intermediate-angle DCS remarkably well. To test the potentiality of the present approximation application should be made to targets possessing stronger nonspherical potential than hydrogen.

ACKNOWLEDGMENTS

We would like to thank Professor N. C. Sil, Dr. A. N. Basu, and Dr. P. Mandal for valuable discussions.

[1]T. Chang, R. Poe, and P. Roy, Phys. Rev. Lett. **31**, 1097 (1973).

[2]P. K. Bhattacharyya and A. S. Ghosh, Phys. Rev. A **12**, 480 (1975).

[3]R. Glauber, in *Lectures in Theoretical Physics, Summer Institute for Theoretical Physics, University of Colorado, Boulder, 1958,* edited by W. Brittin and L. G. Duncan (Interscience, New York, 1959), Vol. 1, p. 315; E. Gerjuoy and B. K. Thomas, Rep. Prog. Phys. **37**, 1345 (1974); J. Callaway, Adv. Phys. **29**, 771 (1980).

[4]Yu. D. Oksyuk, Zh. Eksp. Teor. Fiz. **49**, 1261 (1965) [Sov. Phys.—JETP **22**, 873 (1966)].

[5]N. F. Lane, Rev. Mod. Phys. **32**, 29 (1980).

[6]P. K. Bhattacharyya and A. S. Ghosh, Phys. Rev. A **14**, 1587 (1976).

[7]P. K. Bhattacharyya, K. K. Goswami, and A. S. Ghosh, Phys. Rev. A **18**, 1865 (1978).

[8]P. K. Bhattacharyya and K. K. Goswami, Phys. Rev. A **26**, 2592 (1982).

[9]P. K. Bhattacharyya and K. K. Goswami, Phys. Rev. A **28**, 713 (1983).

[10]P. K. Bhattacharyya and A. S. Ghosh, Phys. Rev. A **12**, 1881 (1975); P. K. Bhattacharyya and D. K. Syamal, *ibid.* **29**, 1140 (1984).

[11]P. K. Bhattacharyya and D. K. Syamal, Phys. Rev. A **30**, 126 (1984).

[12]M. A. Brandt, D. G. Truhlar, and F. A. Van-Catledge, J. Chem. Phys. **64**, 4957 (1976).

[13]K. Onda and D. G. Truhlar, J. Chem. Phys. **72**, 5249 (1980).

[14]J. O'Connell and N. F. Lane, Phys. Rev. A **27**, 1893 (1983).

[15]N. T. Padial and D. G. Norcross, Phys. Rev. A **29**, 1742 (1984).

[16]R. J. W. Henry and N. F. Lane, Phys. Rev. **183**, 221 (1969).

[17]S. Hara, J. Phys. Soc. Jpn. **22**, 710 (1967).

[18]S. C. Wang, Phys. Rev. **31**, 579 (1928).

[19]S. Fraga and B. J. Ransil, J. Chem. Phys. **35**, 1967 (1961). See Table II.

[20]K. Takayanagi and Y. Itikawa, in *Advances in Atomic and Molecular Physics,* edited by D. R. Bates and I. Esterman (Academic, New York, 1970), Vol. 6, p. 105.

[21]Recently, Morrison and co-workers have shown that the adiabatic approximation fails near the threshold for rotational and vibrational excitations: A. N. Feldt and M. A. Morrison, Phys. Rev. A **29**, 401 (1984); M. A. Morrison, A. N. Feldt, and B. C. Saha, *ibid.* **30**, 2811 (1984).

[22]A. C. Roy and N. C. Sil, J. Phys. B **12**, 497 (1979).

[23]M. E. Riley and D. G. Truhlar, J. Chem. Phys. **63**, 2182 (1975).

[24]D. A. Liberman, Phys. Rev. **171**, 1 (1968).

[25]M. A. Morrison and L. A. Collins, Phys. Rev. A **17**, 918 (1978).

[26]For different methods usually employed for the calculations of polarization potential see D. G. Truhlar, D. A. Dixon, and R. A. Eades, J. Phys. B **12**, 1913 (1979); Onda and Truhlar, Phys. Rev. A **22**, 86 (1980); M. A. Morrison, Aust. J. Phys. **36**, 239 (1983); M. A. Morrison, T. L. Gibson, and D. Austin, J. Phys. B **17**, 2725 (1984); T. L. Gibson, M. A. P. Lima, K. Takatsuka, and V. McKoy, Phys. Rev. A **30**, 3005 (1984) and references therein. See also Ref. 5.

[27](a) N. F. Lane and R. J. W. Henry, Phys. Rev. **173**, 183 (1968); (b) S. Hara, J. Phys. Soc. Jpn. **27**, 1262 (1969).

[28]T. L. Gibson and M. A. Morrison, J. Phys. B **15**, L221 (1982); Phys. Rev. A **29**, 2497 (1984).

[29]D. G. Truhlar and F. A. Van-Catledge, J. Chem. Phys. **69**, 3575 (1978); R. A. Eades, D. G. Truhlar, and D. A. Dixon, Phys. Rev. A **20**, 867 (1979); M. A. Morrison and P. J. Hay, *ibid.* **20**, 740 (1979); K. Onda and A. Temkin, *ibid.* **28**, 621 (1983).

[30]D. G. Truhlar, K. Onda, R. A. Eades, and D. A. Dixon, Int. J. Quantum Chem. Symp. **13**, 601 (1979).

[31]W. J. Carr, Jr. and A. A. Maradudin, Phys. Rev. **133A**, 371 (1964); W. J. Carr, Jr., R. A. Coldwell-Horsfall, and A. E. Fein, *ibid.* **124**, 747 (1961).

[32]W. Kohn and L. H. Sham, Phys. Rev. **140A**, 1133 (1965).

[33]J. P. Perdew and A. Zunger, Phys. Rev. B **23**, 5048 (1981).

[34]M. A. Morrison, Comput. Phys. Commun. **21**, 63 (1980); G. B. Schmid and D. W. Norcross, *ibid.* **21**, 79 (1980); W. F. Weitzel, T. L. Gibson, and M. A. Morrison, *ibid.* **30**, 151 (1983).

[35]L. Wolniewicz, J. Chem. Phys. **45**, 392 (1966); W. Kolos and L. Wolniewicz, *ibid.* **46**, 1426 (1967).

[36]W. R. G. Barnes, P. J. Bray, and N. F. Ramsey, Phys. Rev.

94, 983 (1954).
[37]S. K. Srivastava, A. Chutjian, and S. Trajmar, J. Chem. Phys. **63**, 2659 (1975).
[38]M. Fink, K. Jost, and D. Hermann, Phys. Rev. A **12**, 1374 (1975).
[39]B. van Wingerden, E. Weigold, F. J. de Heer, and K. J. Nygaard, J. Phys. B **10**, 1345 (1977).
[40]T. W. Shyn and W. E. Sharp, Phys. Rev. A **24**, 1734 (1981).
[41]S. Trajmar, D. F. Register, and A. Chutjian, Phys. Rep. **97**, 219 (1983).
[42]D. G. Truhlar and J. K. Rice, J. Chem. Phys. **52**, 4480 (1970); **55**, 2005(E) (1971), and references cited therein.
[43]S. Trajmar, D. G. Truhlar, and J. K. Rice, J. Chem. Phys. **52**, 4502 (1970); **52**, 4502(E) (1970).
[44]A. L. Ford and J. C. Browne, Chem. Phys. Lett. **20**, 284 (1973) and references therein.
[45]S. P. Khare and B. L. Moiseiwitsch, Proc. Phys. Soc. London **85**, 821 (1965).
[46]D. G. Truhlar and J. K. Rice, Phys. Lett. **47A**, 372 (1974).
[47]S. P. Khare and P. Shobha, J. Phys. B **7**, 420 (1974).
[48]P. Gupta and S. P. Khare, J. Chem. Phys. **68**, 2193 (1978).
[49]J. T. J. Huang and F. T. Chan, Phys. Rev. A **15**, 1782 (1977).
[50]T. T. Gien, Phys. Lett. **68A**, 33 (1978).
[51]A. Jain, A. N. Tripathi, and M. K. Srivastava, Phys. Rev. A **20**, 2352 (1979).
[52]B. L. Jhanwar, S. P. Khare, and M. K. Sharma, Phys. Rev. A **22**, 2451 (1980).
[53]V. L. Narasimham, A. S. Ramachandran, and C. S. Warke, Phys. Rev. A **23**, 641 (1981); **26**, 2270(E) (1982).
[54]B. L. Jhanwar, S. P. Khare, and M. K. Sharma, Phys. Rev. A **26**, 1392 (1982).
[55]K. J. LaGattuta, Phys. Rev. A **21**, 547 (1980).
[56]D. G. Truhlar and M. A. Brandt, J. Chem. Phys. **65**, 3092 (1976).
[57]K. L. Bell, J. Phys. B **14**, 2895 (1981).
[58]G. Staszewska, D. W. Schwenke, and D. G. Truhlar, J. Chem. Phys. **81**, 335 (1984).
[59]D. G. Truhlar, R. E. Poling, and M. A. Brandt, J. Chem. Phys. **64**, 826 (1976).
[60]S. K. Srivastava, R. I. Hall, S. Trajmar, and A. Chutjian, Phys. Rev. A **12**, 1399 (1975).
[61]F. A. Gianturco, U. T. Lamanna, and N. K. Rahaman, J. Chem. Phys. **68**, 5538 (1978). In this paper only the asymptotic part of e-H_2 potential is considered.
[62]J. C. Tully and R. S. Berry, J. Chem. Phys. **51**, 2056 (1969).
[63]L. A. Collins, W. D. Robb, and M. A. Morrison, Phys. Rev. A **21**, 488 (1980).
[64]T. L. Gibson and M. A. Morrison, J. Phys. B **14**, 727 (1981).
[65]L. A. Collins and M. A. Morrison, Phys. Rev. A **25**, 1764 (1982).
[66]To be precise, for the computation of $I(1\rightarrow 3,\theta)$ at 40 eV polarization potentials with exponential (Ref. 56) and Buckingham-type (Ref. 17) cutoff functions, *ab initio* polarization potentials of Lane and Henry [Ref. 27(a)] and Truhlar *et al.* (Ref. 26), and the correlation-polarization potential of the present study have been considered so far.
[67]This is also true for the *ab initio* polarization potential of Gibson and Morrison (Ref. 28); we have checked it in a test calculation with potential model B-GM-$H(I_p)$ (according to our convention).